CHAPTER 11
APPLICATION OF GROUND PENETRATING RADAR TO INVESTIGATIONS OF THE STRATIGRAPHY, STRUCTURE, AND HYDROLOGY OF ST. CATHERINES ISLAND

R. Kelly Vance, Gale A. Bishop, Fredrick J. Rich, Brian K. Meyer, and Eleanor J. Camann

Ground penetrating radar (GPR) is a high-resolution geophysical tool for relatively shallow imaging of soil, sediment, rock, or ice using electromagnetic waves of 10 to 1000 MHz frequency. For detailed descriptions and discussion of operational theory and technique, the works of Daniels (2004) and Baker, Jordan, and Pardy (2007) and web resources of Olhoeft (2006) and Conyers (2009) are recommended. The equipment and technique have a prolonged history of development beginning with the application of electromagnetic signals to the detection of subsurface features in 1904, followed by the use of pulsed techniques by 1926, that were soon applied to investigation of ice, sand, rock, coal, salt, and water in the 1930s (Daniels, 2004). Lunar exploration in the 1970s promoted improvement and compaction of equipment toward the GPR systems used today in a broad range of noninvasive applications to archaeology, cultural resource management, forensic investigation, mine detection, determination of road, bridge, and building integrity, crevasse detection on glaciers, detection of buried wastes, detection of underground storage tanks and conduits, and the subsurface geological investigation of stratigraphy, structures, and hydrology (Sharma, 2002; Daniels, 2004; Baker, Jordan, and Pardy, 2007).

Geophysical surveys using GPR, magnetometer, and resistivity have been applied to archaeological investigations on St. Catherines Island for more than two decades (Garrison and Baker, 1985; May, 1985; Thomas, 1987; Sanger and Thomas, 2010). The St. Catherines Island investigations have become an operational model for archaeological site conservation by maximizing the use of noninvasive geophysical surveys and other techniques to focus and limit excavation (David Hurst Thomas and Royce Hayes, personal commun., 2007; Bishop, Vance, and Meyer, 2007). GPR remains an important noninvasive tool for archaeologists in reconnaissance of large buried structures or for high-precision, closely spaced profile grid lines in surveys that allow processing of the data into horizontal planes ("time slices") or three-dimensional images. The second method accommodates the need for documenting spatial relationships at sites and lateral variation within horizons. Application of geophysics to the geological investigation of St. Catherines Island has been relatively limited and the geological framework for understanding the island evolution has been built on the application of fundamental geological principles and traditional field and laboratory techniques to the sediments and sedimentary rock via limited surface exposure, trenching, augering, and vibracoring (Bishop et al., chap. 3 and chap. 10, this volume; Thomas, 2009; this volume, chaps. 1, 3, and 10).

In 2005, the Department of Geology and Geography at Georgia Southern University acquired a MALA GPR system with a Ramac X3M controller that can be paired with 100 MHz, 250 MHz, 500 MHz, or 800 MHz antennae. These are shielded antennae that incorporate both transmitter and receiver in one unit at fixed spacing. The controller-antenna system can be used for GPR profiling in either cart or sled mode for the 500 MHz and 250 MHz antennae, but requires sledding for the 100 MHz antenna. A laptop computer, or the MALA Ramac monitor can be used to calibrate and configure the system and record

data and profile markers. The compact, durable, heat- and dust-resistant construction and simple operation make the Ramac monitor preferable to the laptop for prolonged field use. The system is powered by a lithium-ion battery that provides approximately five hours of use. A second, fully charged backup battery ensures a full day of use. GPR profile distance is recorded internally using a wheel odometer attached to the antenna or cart or by using a hip chain system. A time triggering mode is also an option if conditions do not allow direct measurement by odometer or hip chain. Survey data recorded in the monitor can be downloaded to a flash drive or through USB cable to a laptop or desktop computer for processing with MALA software.

Access to GPR equipment allows nondestructive geological exploration of the shallow subsurface of St. Catherines Island. Geological exploration, interpretation, and representation of stratigraphy and structure rely heavily on a cross-sectional perspective; consequently, most of the GPR surveys described here were conducted by reflection profiling to develop subsurface cross sections of the geology. The depth of penetration and resolution of subsurface features depends largely on the antenna, the sediment or rock type and density, and the amount and salinity of groundwater. Under identical conditions, lower frequency antennae achieve the greatest penetration, but with lower resolution. Higher frequency antennae provide the best resolution, but least penetration. Under optimum conditions the 100 MHz antenna has the capability to resolve features of 50–60 cm thickness, the 250 MHz antenna can resolve features of 2 cm thickness, the 500 MHz antenna can resolve features of 1 cm thickness, and the 800 MHz antenna can resolve features between 1 cm and 0.6 cm thickness. On St. Catherines Island, the maximum penetration with return of ground radar energy occurs in dry sand. Groundwater increases the dielectric constant and decreases velocity of radar waves. Saltwater saturation results in complete loss of return signal and the presence of clay rapidly attenuates radar energy (Daniels, 2004). Although these characteristics limit effective depth of the radar profile, they also provide indirect information or at least constrain interpretations of subsurface geology.

Vance and Bishop began experimenting with the MALA system and GPR applications on St. Catherines Island in 2005, gradually exploring the potential of the system with the assistance of coworkers, students, and family using various combinations of antennae, settings, and adjustments for different applications. Results presented here represent some of the applications of the system and implications for geology of the island. The profiles shown or discussed provide a framework that may be used to focus future exploration or to constrain the current interpretations of subsurface geology.

GPR APPLICATIONS ON ST. CATHERINES ISLAND

Sea Turtle Nests and GPR

Sea turtle conservation work requires an annual monitoring presence on St. Catherines Island and includes a teacher education program (see http://scistp.org/) on the island; consequently, it was natural to run an early GPR experiment on sea turtle nests. Gale Bishop noted the difficulty in locating egg chambers produced by the rare leatherbacks nesting on the St. Catherines beach and wondered if the egg chamber could be detected with GPR (Bishop et al., this volume, chap. 13: fig. 13.4). To test this possibility we used a loggerhead nest in which the egg chamber had been located and ran profiles with 0.5 ft spacing over a 12 ft by 17 ft area that enclosed the body pit of the turtle nest. An 800 MHz antenna was selected for this project to achieve the maximum resolution possible for this shallow feature. We smoothed the sand surface of the body pit to avoid changes in energy coupling produced by surface irregularities. The upper portion of the profiles exhibit what appears to be the broadly concave cross section of the body pit. The profile (fig. 11.1) is one of two profiles that exhibited a broad hyperbolic reflection above a zone with a minimal or weak reflection. This feature coincides with the actual position of the egg chamber. The hyperbolic reflection probably results from radar wave interaction with the compacted sand filling above the eggs and/or the margins of the egg chamber. The weak signal under the hyperbolic reflector may be due to energy loss in the soft mass of turtle eggs (see Bishop et al., this volume, chap. 13: fig. 13.7A, B). The experiment suggests that a leatherback egg chamber could be detected with the 800 MHz antenna. The subtle nature of the nest signature would probably require leveling of the body pit surface to avoid the change in radar energy coupling effects or better yet, laying a smooth, firm, radar

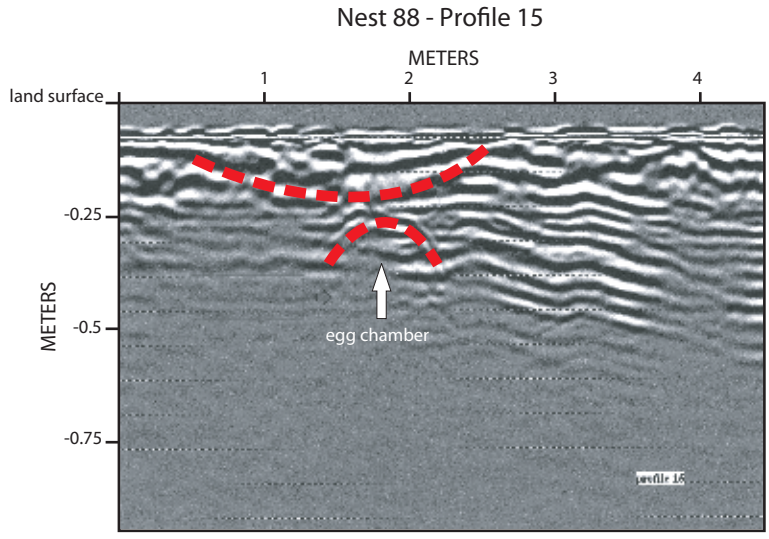

Fig. 11.1. GPR profile (800 MHz) across a loggerhead sea turtle nest. The upper highlights outline the margin of the concave reflections attributed to the body pit. The lower highlights mark the broad hyperbolic reflections that are probably produced by packing of sand into and over the egg chamber and/or the egg chamber walls. Note truncation of reflectors at the margins of the body pit and egg chamber.

transparent sheet over the surface. The 800 MHz antenna is generally limited to penetration depths <1 m but is capable of centimeter-scale resolution. It is designed largely for mapping hidden structural features in walls and floor (rebar, conduits, fractures, voids) but has the potential for exploring fine beach stratigraphy, heavy mineral sand distribution, burrow networks, and localized high-resolution archaeological work. This experiment also indicated that the small odometer wheel would need to be modified for any extended beach work to keep loose sand out of the wheel axles and to increase the frictional contact between the smooth plastic wheel and sand. Using a hip chain anchored at profile stakes would be another very slow option.

Exploring the Subsurface Structure and Stratigraphy

The road network on St. Catherines Island provides an opportunity for both northwest-southeast profiles across the short axis of the island and northeast-southwest longitudinal profiles. The marked road junctions on the island map prepared by Timothy Keith-Lucas and others provide useful references for profile endpoints and internal markers. Over 20 km of GPR profiles (see table 11.1) were acquired from 2005 to 2009.

Most of our work has been conducted by two-person teams towing a 100 MHz antenna with attached odometer wheel behind a John Deere Gator ATV with the GPR operator sitting in the back of the ATV using a shoulder-mounted harness for the monitor and battery (fig. 11.2). Initial profiles conducted with a time window of ~290 ns indicated a very strong signal return in the higher, dryer parts of the island, so the time window was opened to ~490 ns to take advantage of conditions that allowed profiling to depths of 7–10 m. Processing of the GPR profiles shown here is limited to minor band pass filtering and time gain adjustment. Most of the profile surfaces had little relief, negating the necessity for topographic corrections.

Velocity of the radar waves may be calculated from diffraction hyperbolae using the MALA Radar Explorer software program. A velocity range from 4 cm/ns to 13 cm/ns was determined by this method. A velocity of 5 cm/ns was used as an average as it gave reasonable agreement with the thickness of sand exposed at Yellow Banks

Bluff and limited data from vibracoring (Bishop et al., this volume, chap. 10). It is emphasized that the depth profile scale will shift markedly if the velocity is changed; consequently, GPR profiles are often displayed with two-way travel time in nanoseconds on the vertical scale. Profile depth accuracy can be improved by subdividing the profile into layers of differing velocity and

TABLE 11.1
Ground Penetrating Radar Profile Inventory

File-year	Road junctions → direction	Antenna/ time window
OMPF-06	Jct. 12 → Picnic Bluff	100MHz/shallow
OMPG-06	Jct. 13 → Magnolia Bluff	100 MHz/shallow
OMPH-06	Jct. 13 → Jct. 64	100 MHz/shallow
OMPI-06	Jct. 64 → end Engineers Road	100 MHz/shallow
OMPJ-06	Jct. 26 → Jct. 52	100 MHz/shallow
OMPK-06	Jct. 52 → Jct. 50	100 MHz/shallow
OMPO-07	North end Flag Pond on Jungle Road →Jct. 35	100 MHz/medium
OMPP-07	Jct. 35 → Jct. 32	100 MHz/medium
OMPQ-07	Jct. 32 → Jct. 31 → Jct. 57	100 MHz/medium
OMPR-07	Jct. 57 → Jct. 52 → end near State Pond	100 MHz/medium
OMPT-07	Jct. 13 → Jct. 12 → Jct. 10	100 MHz/medium
OMPU-07	Jct. 10 → Jct. 61 → Jct. 60	100 MHz/medium
OMPV-07	Jct. 60 → last Jct. on Engineers Road	100 MHz/medium
OMP2-07	Jct. 26 → Jct. 71 → Jct. 80	100 MHz/medium
OMP3-07	Jct. 80 → Jct. 68 → 78	100 MHz/medium
OMP4-07	Jct. 68 → Jct. 66 → Jct. 65	100 MHz/medium
OMP5-07	Seaside Dock → Jct. 18 → Jct 45 → Jct. 65 → Jct. dock on Walburg Creek	100 MHz/medium
OMP6-07	Magnolia Bluff → Jct. 13 → Jct. 64 → pasture on north side of barn	100 MHz/medium
OMP7-07	Jct. 57 → Jct. 72 → Jct. 87 → Jct. 83	100 MHz/medium
OMP1-08	Northeast end of Cracker Tom Hammock → Jct. 29 → Jct. 28 → Jct. 53 → Jct. 54 → Jct. 59 → Jct. 58 → Jct. 54 → Jct. 31 → Jct. 29	250 MHz/deep
OMP1-09	Jct. 62 → Jct. 60 → north loop → Jct. 10	100 MHz/medium
OMP3-09	Jct. 60 → Jct. 61 → Jct. 10	250 MHz/deep
OMP4-09	Windmill Jct. → Jct. 13 → Jct. 12 → Sand Pit Road Jct.	250 MHz/deep
OMP5-09	Jct.59 → Jct. 58	250 MHz/deep
OMP6-09	South Pasture 90° to Jct. 59-58	250 MHz/deep
OMP7-09	South Pasture 90° to Jct.59-58	250 MHz/deep
OMP9-09	Jct. 60 → Jct. 61 → Jct. 10	100 MHz/deep

Fig. 11.2. GPR reflection profiling system used on St. Catherines Island to obtain over 20 km of profiles along the island road network. This MALA GPR system includes a 100 MHz antenna with attached control box and odometer wheel towed by a John Deere Gator ATV. Operator (R.K. Vance) sits with monitor and battery pack in a shoulder-mounted harness linked to control box by serial cable and power line (photograph by Lisa Vance).

reprocessing it; however, this treatment is best suited to short profile segments.

Profiles may be treated by identification of radar surfaces and by grouping radar reflection elements into packages or associations and radar facies (Jol and Smith, 1991; Hugenholtz, Moorman, and Wolfe, 2007). The ground radar waves react to changes in subsurface physical properties that may or may not coincide with bedding surfaces or structures. Obtaining ground truth or hard geological data via surface exposures, trenching, augering, and coring is essential for accurate interpretation of the radar surfaces, facies, and elements. This chapter includes interpretation of radar elements and facies in terms of sedimentary bedforms and associations. These interpretations are constrained by geological setting, comparison with bedforms characteristic of similar geological settings, available ground truth, and comparison with published GPR profiles; however, it should be emphasized that these are *interpretations* of radar reflections and alternative interpretations may be viable.

Holocene-Pleistocene Terrain Boundaries

The younger Holocene accretionary terrains, with characteristic ridge and swale topography (see this volume, chap. 3: figs. 3.2 and 3.5) provide a frame of reference for recognition of subsurface beach ridge bedforms in older deposits (fig. 11.3). The GPR profiles provide a subsurface geophysical view of the contact between the younger Holocene accretionary terrains and the Pleistocene core of the island. Figure 11.4A is a spliced excerpt from the west end of profile OMPP-06 and the east end of profile OMPQ-06. This segment begins on the west side of a salt marsh 87 m east of Jct. 32 and extends west of Jct. 31. Notable features on the profile include the signal attenuation on the east end of the profile due to the saltwater wedge extending from the marsh. Saltwater saturation limits the GPR to depths of less than 3 m under most of the younger Holocene ridges. The initial profile segment trends southeast to northwest across the strike of the Holocene beach ridges. Heavy dashed lines on the profile are major radar surfaces. At the east end of the profile the uppermost radar surface separates an upper facies of eastward dipping subparallel planar radar reflections or elements from an older, steeper (Pleistocene?) facies characterized by more steeply dipping sigmoidal reflections. The upper facies (Holocene?) changes westward into subhorizontal flattened concave to

convex reflection elements that overlie southward dipping sigmoidal forms. The approximate dip direction of the reflections is obtained at Jct. 32 where the profile turns sharply northeast—note change in apparent dip of the upper and lower facies elements.

The upper facies elements appear discordant to those of the underlying facies. The upper facies also dips southeastward (see east side of Jct. 32 on fig. 11.4A) and thickens toward the marsh, features compatible with sediment filling the marsh or swale. The upper facies thins westward to <1 m near Jct. 31. The upper facies elements overlie and locally truncate middle facies elements. The sigmoidal radar elements of the underlying facies suggest a prograding (regressive) beach system with some periods of transgression marked by lower angle elements truncating and overlying older elements (Johnston, Thompson, and Baedke, 2007). The upper facies may represent overwash deposits and dune ridges and swales that have been flattened over time. The 100 MHz profiles have a 5× exaggeration that compresses features; consequently, reflections or interpreted bedforms with an apparent 30° dip are actually ~6°. The reflections of the middle beach facies exhibit tangential contacts with reflections of an underlying facies composed of horizontal, parallel to subparallel elements including one or two strong reflectors capping weak reflections or bedforms. The weak reflections are interpreted as mud and sandy mud with possible saltwater saturation at depth. These parallel bedforms or reflections constitute an additional lower radar facies. Two strong reflecting surfaces (referred to as the basal reflectors) appear to be a fairly persistent radar surface that may serve as a stratigraphic marker. Road Jct. 32 is probably very close to the boundary between the island core and the younger Holocene accretionary terrains. The base of the

Fig. 11.3 (*right*). True-color image (2005) of St. Catherines Island showing Pleistocene core and Holocene accretional terrains (aerial image source USDA, NAIP 2005). Locations A–Z are profile segment sites illustrated in figs. 11.4–11.16.

upper facies appears to truncate the middle facies between Jct. 32 and the marsh. The profiles also suggest that some of the younger (eolian portion) sediments overlap and cover at least part of the island core; however, there is no way to verify age equivalence with GPR alone.

The reflector marked with dots in the upper 1.5 m of the profile may be humate concentrations or another pedogenic feature such as B horizon development with iron oxide concentrations. The contact between the white eolian "sugar sand," which is the C horizon of the uppermost soil profile of Vento and Stahlman (chap. 4, this volume) and the hard humic A horizon of an underlying paleosol is a another possibility; Vento and Stahlman note a lack of lateral continuity in specific soil horizons. This shallow reflector is best developed in higher standing portions of the island and may be related to former water tables or soil horizon development. This upper reflector will be referred to here as the humate reflector or pedogenic reflector. Similar looking reflections are identified as water tables in some GPR studies; however, the St. Catherines reflectors are too shallow in areas where the water table was determined and vibracore and auger work display humate or changes in iron oxide concentrations that appear to more closely match this feature. In a few profiles this reflector appears to be superimposed on possible bedforms, favoring an origin related to shallow water table redox gradients or some pedogenic process. This GPR reflector is observed in both the Pleistocene core of the island and some of the adjacent late to middle Holocene beach ridges that are accreted against the Pleistocene core. This observation is in agreement with Vento and Stahlman's observations on more oxidation and humate development in C horizons of the late-middle Holocene terrain. In one GPR profile in the island core, the humate or pedogenic reflector is actually offset by a minor fault indicating brittle behavior consistent with iron oxide or humate cemented sands. The apparent overlap (fig. 11.4B) of the younger upper facies succession onto the older island core beach facies is compatible with investigations and interpretations (Vento and Stahlman, chap. 4, this volume) of the northern end of the island where Holocene paleosols and/or eolian deposits occupy the upper 2–3 m of Yellow Banks Bluff.

A transect across Cracker Tom Causeway onto the island core provides another look at the boundary between younger accretionary terrain and the island core. This profile (fig. 11.4B) was conducted with a 250 MHz antenna and the scale exaggeration of ~5× compresses the cross section and steepens apparent dips. The 250 MHz antenna can resolve thinner bedforms, but also produces more noise and clutter from near-surface diffraction hyperbolae generated by roots and shells. The transect segment shown begins on the causeway over the last major salt marsh east of Jct. 29. The saltwater attenuates the radar signal wedge from 1230 to 1265 m on the profile. Marsh is also present on the south side of the road at 1322–1335 m, but the water appears to be brackish to fresh and the signal is not completely attenuated. The 1235–1320 m section runs north to south subparallel to the ridge, then bends sharply northwest across ridge strike from 1325 to 1351 m (Jct. 29). The steeper portion of the bedforms near Jct. 29 dip ~6° (corrected) east to southeast. The change to subhorizontal bed orientation at Jct. 29 coincides with a profile turn to the north subparallel to ridge strike. An approximate base of the Holocene is suggested (red on fig. 11.4B) on the marsh side of the profile using the Cracker Tom vibracore data (Bishop et al., 2009b; this volume, chap. 10) and apparent truncation of strata as a guide. The boundary between the younger Holocene-dominated terrain and the older island core is probably at 1347 m on the profile. At this location near Jct. 29, there are marked changes in reflection intensity and attitude, and the pedogenic reflector (dotted on fig. 11.4B) is well developed on the island core side (contrast with Cracker Tom Hammock in fig. 11.5B, lower). Part of the dramatic change in reflection angle and appearance near Jct. 29 is due to the change in profile strike from ridge-perpendicular to ridge-parallel; however, the collective change in radar reflection and intensity favors this location as the boundary and agrees well with surface topographic features. If Holocene dune ridges override the Pleistocene core here, as suggested in the southeastern profiles and the Yellow Banks soil chronology of Vento and Stahlman (chap. 4, this volume), the Pleistocene and Holocene beach and ridges were nearly parallel as the strike parallel profile section (fig. 11.4B, lower: 1350–1405 m) has consistent subhorizontal, subparallel reflections. Figure 11.5A (upper) shows a northeast-southwest profile segment C–C′ between jcts. 53 and 54. This profile shows a change in radar facies at approximately 2.5 m depth between an upper facies characterized by wavy subparallel reflections or

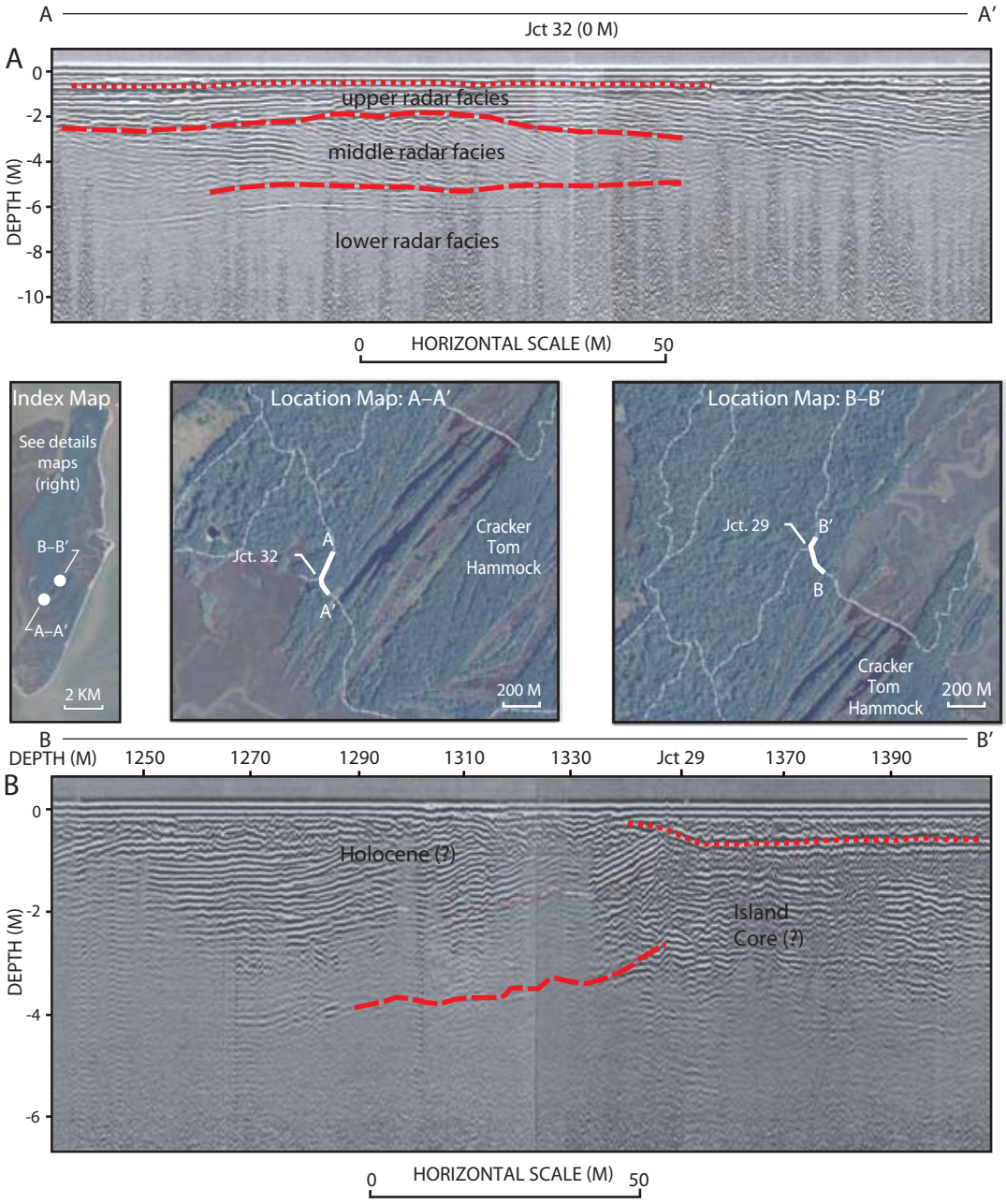

Fig. 11.4. **A,** Profile A–A′: composite (end of OMPP-06, beginning of OMPQ-06) NE-E 100 MHz GPR profile. Road Jct. 32 is at 0 m. Location map above shows profile location and orientation. The upper highlight (dotted line) marks a pedogenic or humate cement reflector. The dashed highlights mark radar surfaces separating upper, middle, and lower radar facies. Reflectors on east side dip toward a salt marsh. **B,** Profile B–B′: segment from OMP1-08, 250 MHz profile from west side of causeway (~90° to ridges) over Cracker Tom Marsh to Jct. 29 (1350 m) turning subparallel to beach ridge strike on the island core. Highlight is suggested contact between Holocene accretionary terrain and island core (aerial image source USDA, NAIP 2005).

bedforms and a complex underlying facies bearing multiple reflection elements. The lower facies includes some of the sigmoidal clinoform radar elements that characterize prograding (regressive) beach systems (Johnston, Thompson, and Baedke, 2007). The upper wavy facies is overlain by horizontal reflectors in the upper 2 m, perhaps representing pedogenic structure superimposed on eolian deposits.

Cracker Tom Hammock contains a relatively thick (>3 m) sequence of sand (fig. 11.5B, lower: 572–695 m) and satellite images reveal a high-standing landscape more mature in appearance than most of the Holocene accretionary terrains. Chowns et al. (2008) noted the apparent maturity of Cracker Tom Hammock in the context of surrounding accretionary terrains. Vibracoring on the shoulders of the subdued ridges in the marsh on the north side of Cracker Tom Causeway, between Cracker Tom Hammock and the island core, penetrated a disconformity (Booth, Rich, and Bishop, 1999; Linsley, Bishop, and Rollins, 2008). Dating of organic components above and below the disconformity (Rich and Booth, this volume, chap. 6; Bishop et al., this volume, chap. 10) confirms a Pleistocene substrate for the Holocene ridges in the marsh. The ridge pattern on Cracker Tom seems nearly parallel to that visible along the core margin across the salt marsh, while the lower standing ridges in the intervening marsh are discordant to the ridges of both Cracker Tom and the island core margin. These features encourage speculation in the search for a viable explanation. If there is a significant Holocene eolian cover on the eastern island core (chap. 4, this volume), could the highest ridges on Cracker Tom and the ridges on the margins of the island core be correlative younger Holocene dune deposits? Are these deposits age equivalent to the succession that appears to override the core (see fig. 11.4A) along the southeastern end of the island?

What accounts for the lower elevation of the ridges between Cracker Tom and the island core? The interior margin of Cracker Tom Hammock is particularly sharp. Did the former course of the Ogeechee (Chowns et al., 2008) or another stream carve a channel between Cracker Tom and the island core, removing the upper layer of Holocene dune and beach deposits to expose the top of the underlying ridges? Could the high standing Cracker Tom Hammock and the next high standing accretionary ridge package to the east be the southern tail of Guale Island (chap. 3, figs. 3.2 and 3.5) isolated by shifting channels or tidal creeks? Another possible explanation for the low elevation of the ridges in the marsh between Cracker Tom Hammock and the core is deposition of the beach ridge system during a period of lower sea level and/or diminished sediment supply (see Bishop et al., this volume, chap. 10). This explanation requires that the similarities in orientation and elevation of the ridges of Cracker Tom Hammock and the core are either a coincidence or represent the return to nearly identical conditions of sea level, longshore current, and sediment supply. The adequate resolution of these questions will require more ground truth (vibracore, trenching) and sedimentological evaluation coupled with dating and elevation control. The thick sequence of strata underlying Cracker Tom Hammock and the relative maturity and stability suggest a rich area of future island exploration for both archaeologists and geologists.

An additional means of producing a topographically subdued beach ridge terrain between a younger, higher terrain (like Cracker Tom) and the island core is offered indirectly by Thomas (chap. 1, this volume) in his discussion of hurricanes and paleotempestology. Just as the barrier islands provide a "mega-breakwater" between the sea and mainland, the young island-fringing accretionary terrains are the first barrier between the island core and sea. If the island was subjected to major hurricane strikes after accretion of the low ridges observed today in Cracker Tom marsh, but prior to accretion of ridges in Cracker Tom Hammock, the wave battering and storm surge from the hurricanes should have flattened the younger, least stabilized beach ridges as well as dunes on the margin of the island core (Bishop and Meyer, this volume, chap. 14: fig. 14.3). A Category 5 hurricane may generate storm surges exceeding 5 m, flooding lower elevations of the island core and beveling and breaching the fringing beach ridges. Perhaps the low-standing ridge systems situated between higher ones represent periods of excessive hurricane activity between quiescent periods. Another low ridge system is located between Cracker Tom Hammock and a higher ridge to the east. Does this package also reflect a period of intense hurricane activity?

Differences in accretionary terrain development should be influenced in large part by a combination of sea level change and inlet shifting as well as changes in sand transport and supply

(Linsley, Bishop, and Rollins, 2008; Bishop et al., 2009a; Bishop et al., chap. 3; Bishop et al., chap. 13; Bishop and Meyer, chap. 14: fig. 14.13; and Rollins and Thomas, this volume, chap. 16). These forces can certainly be combined with some of the possibilities described above to achieve the complex pattern of accretionary terrains observed today along the southeastern flank of St. Catherines Island. Barrier islands are extremely dynamic environments and the rapid rate of recent erosion and accretion on St. Catherines Island is well documented (Bishop and Meyer, this volume, chap. 14: figs. 14.10 and 14.13; Potter, this volume, chap. 7). The interpretation of island features relative to a changing sea level is also complicated by evidence for faults and tectonic activity affecting the strata of the southeastern coastal plain (Bartholomew et al., 2007; Vento and Stahlman, this volume, chap. 4), producing an apparent sea level change (local tectonic uplift or subsidence). The presence of minor faults and joints on St. Catherines Island indicates that tectonic influence should be considered.

South Pasture Disconformity

The 250 MHz profile (OMP1-08) revealed a striking feature along the southwest to northeast road bordering the east side of South Pasture between Jct. 59 and 58. The profile exhibits an apparent disconformity 2–5 m below the present surface, extending from Jct. 59 northward, climbing over a 2 m buried scarp onto sandy strata providing good radar reflections, ~570 m north of Jct. 59. The surface is very irregular and displays over 3 m of relief in some areas. Reflection intensity between the soil and disconformity is very poor. Additional exploration includes another GPR profile (fig. 11.4A, upper profile) between Jct. 59 and 58 to verify results plus two short right-angle profiles that intersect the main profile line in the sand-dominated section (fig. 11.6B, lower profile) and over the disconformity. The additional GPR profiles indicate that the disconformity does extend to the east and climbs northward to ~1–1.5 m depth. The 1–1.5 m depth is approximately the same as the base of the upper facies shown in figure 11.4. Two vibracores were obtained in February 2009 with the assistance of an undergraduate research team (Shannon Ferguson, Jesse DeLaMater, Nick Wieclaw) from Georgia Southern University. One vibracore sited over the disconformity at the 522 m mark on profile OMP5-09 refused penetration at ~3 m depth (~0.4 m added for compaction) and bottomed out in sticky blue-gray mud. Core logging revealed ~2.6 m of sand-dominated upper section underlain by ~10 cm of very dense, blue-gray clay with iron oxide mottling. The lowest 2–3 cm of clay from the base of the core were mixed with fine sand. The other core site over the sand-dominated section at 624 m on profile OMP5-09 penetrated ~2.4 m and logging revealed nothing but sand. A soil auger hole determined the water table at ~2.7 m on the day the profile was conducted. This water table depth indicates that the dense, sticky clay is perching the water table over the disconformity at South Pasture. Water saturation of sand as a perched aquifer above the clay explains the very poor signal return above the disconformity.

What are the origin and significance of this erosional feature? Was the erosional surface a localized product of shifting tidal creek channels along the island's southern margin or a major change in inlet configuration? Is the South Pasture disconformity correlative with the upper disconformity (#2 in Bishop et al., this volume, chap. 10: figs. 10.6 and 10.8) identified in the marsh cores from the St. Catherines Shell Ring vibracore transect? Is the buried scarp (see fig. 11.6A, upper: 545–590 m) an older Holocene equivalent to Wamassee Scarp or Zapala Sound margin (see fig. 3.2; Bishop et al., this volume, chap. 3)? At this time the discovery raises more questions than answers; however, the clay may provide a source of organic material to resolve some of these questions through palynological study and possibly ^{14}C dating.

GPR Transects across the Island Core

The GPR profiles conducted across the northeast-southwest longitudinal axis of the island reveal one or two persistent basal reflectors (fig. 11.7A, B) that can be traced within the core of the island and beneath at least part of the adjacent Holocene accretionary terrains. These reflectors have sharp upper surfaces with underlying horizontal parallel radar reflections or bedforms. The signal strength fades quickly below these markers, suggesting that the reflecting surfaces represent the interface between sand-dominated and clay-dominated strata. These surfaces may be correlative with the Pleistocene mud and marsh sediments identified in vibracore transects at Cracker Tom Causeway and the St. Catherines Shell Ring (Bishop et al., this volume, chap. 10: figs. 10.6 and 10.8). They may

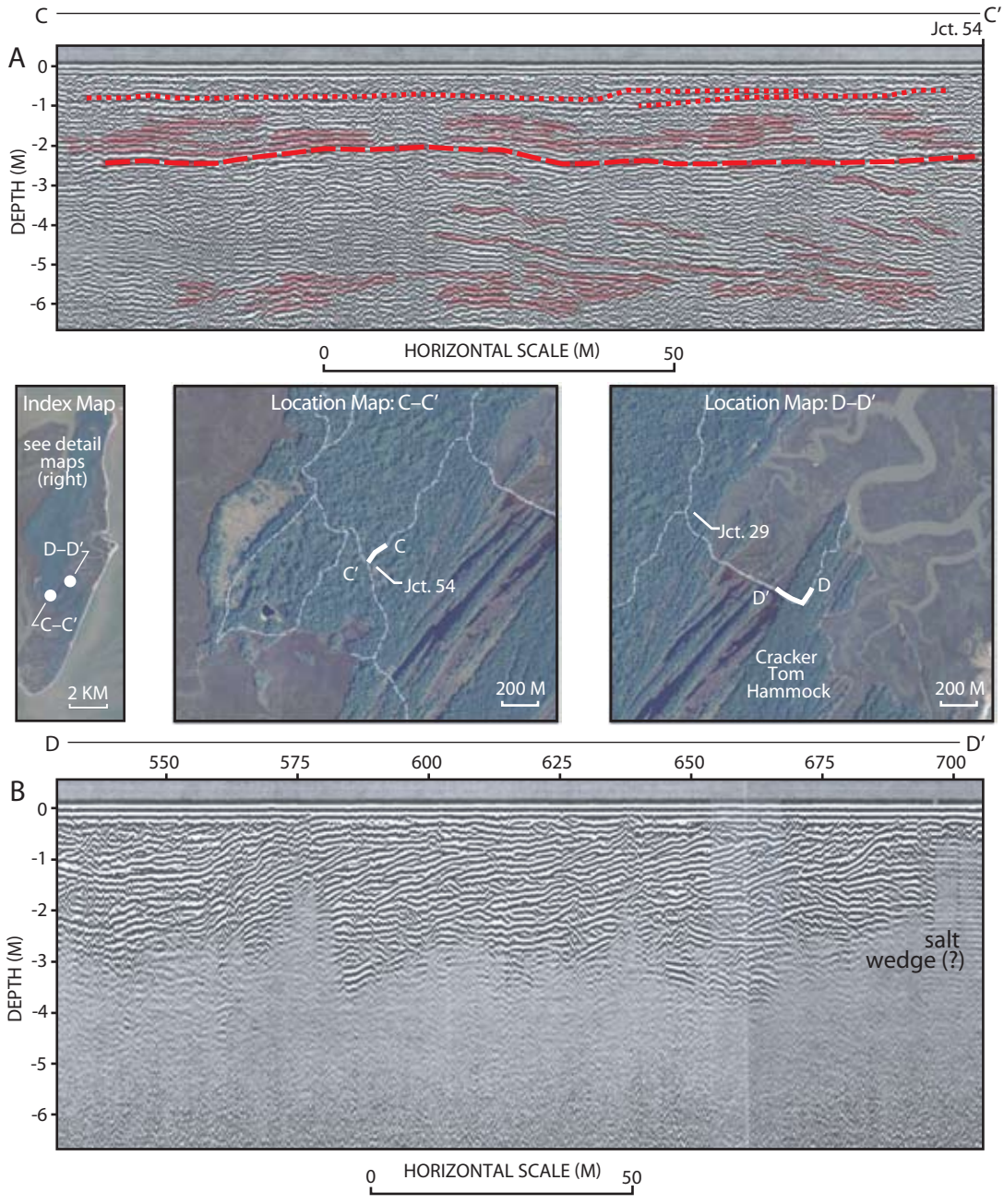

Fig. 11.5. **A,** Profile C–C′: NE to SW 250 MHz profile segment from OMP1-08 between jcts. 53 and 54. Upper pedogenic or humate reflector is marked with dotted highlights; the heavy dashed highlight marks radar surface separating middle horizon facies bearing sigmoidal radar elements from upper facies of wavy radar elements or bedforms. **B,** Profile D–D′: segment of 250 MHz profile OMP1-08 on Cracker Tom Hammock showing reflection change at 565 m, from a ridge parallel profile to ridge perpendicular profile. Note well-developed sigmoidal clinoform radar elements (565–700 m). A saltwater wedge attenuates radar signal sharply on the west end of the profile (aerial image source USDA, NAIP 2005).

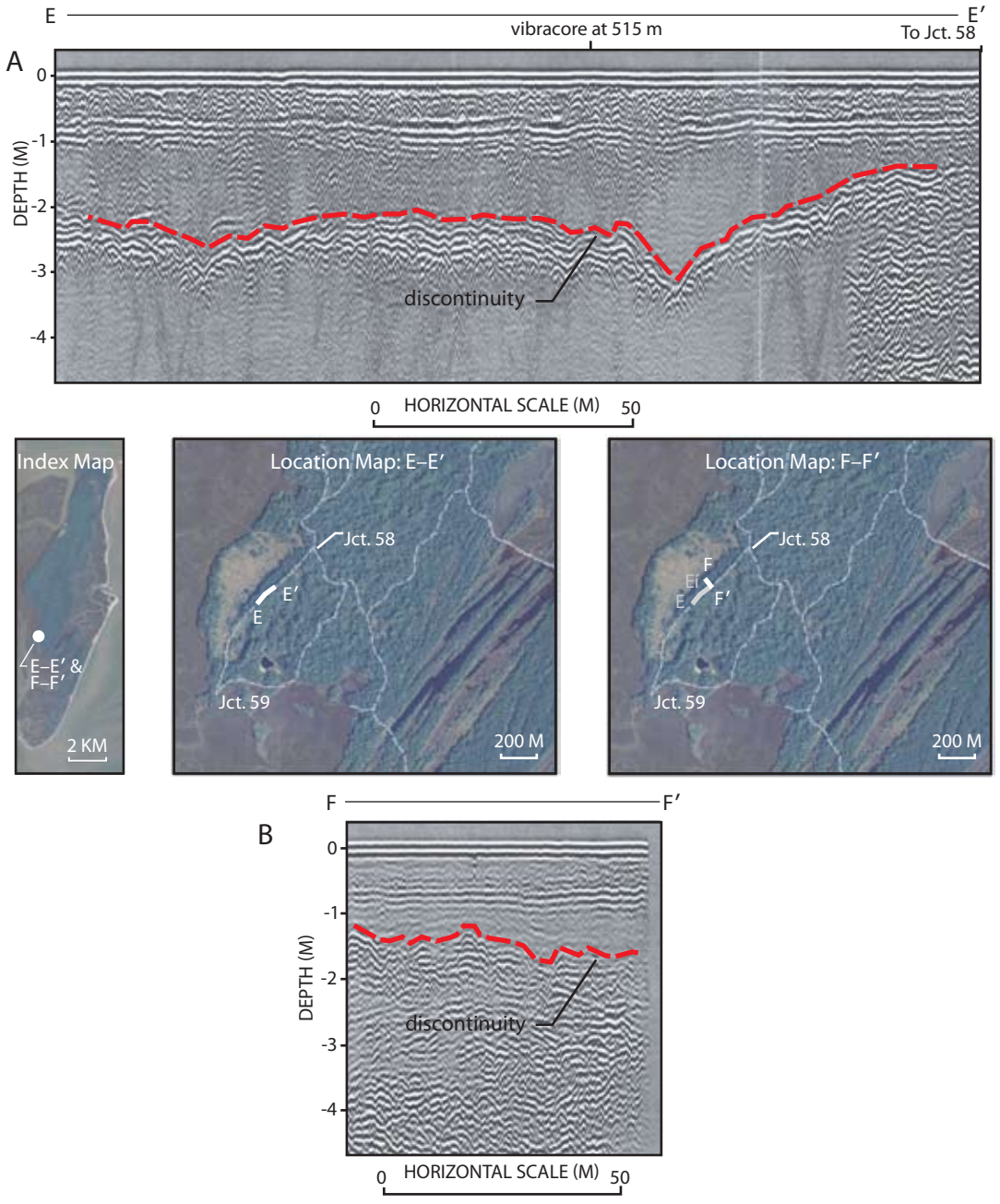

Fig. 11.6. **A,** Profile E–E′: SW-NE 250 MHz profile (OMP5-09 segment between jcts. 59 and 58 at South Pasture. Apparent disconformity with 1–1.5 m of relief "climbs" over a buried scarp onto a sand-dominated succession at the NE end of profile. A 3 m vibracore sited at ~515 m along the profile terminated in dense blue-gray clay. Poor signal in sand above clay is probably due to water saturation. **B,** Profile F–F′: a short W-E 250 MHz profile (OMP7-09) at right angle to that shown in fig. 11.6A confirms irregular surface of disconformity on sand-dominated succession at north end of profile OMP5-09 (aerial image source USDA, NAIP 2005).

also represent hydrologic boundaries between freshwater-saturated strata and saltwater-saturated strata. Locally these reflectors are incised by scours or small channels indicating local disconformity and a higher energy environment. The bedforms or radar elements (probably sand dominated) above the basal mud or muddy sand exhibit tangential bedding relationships with the lower facies reflectors. If the elevation of the basal reflectors is relatively uniform, they provide a good reference marker to gauge the thickness of the overlying sand-dominated strata. The eastern side of the island has ~6–8 m of sandy strata above the basal reflectors that thin westward to a thickness of 2–5 m along the western margin of the island. GPR penetration and data are more limited along the Central Depression or longitudinal axis of the island. This may be due to higher water tables, more clay-rich sediments near the surface, and/or a combination of these features. There are also intermittent zones of poor GPR signal return in the sand-dominated strata east of the Central Depression. Some of these zones may represent buried interdune marshes, swale ponds, or even freshwater ponds rich in clay and organic components.

Figure 11.7A (upper profile) is a northeast-southwest profile segment G–G′ (646–732 m) between Jct. 52 and 71 showing lower planar parallel layers (probable muddy sediments) with strong reflecting horizons at ~5.5 m and 8.5 m depth. The lower planar parallel facies is overlain by a middle facies of radar elements characterized by lower beds dipping gently eastward, forming tangential contacts with the 5.6 m reflector. Radar elements suggesting trough cross-bedded forms are also observed. The eastward-dipping bedforms of the middle facies are overlain by westward-dipping beds suggestive of dune and washover deposits and a 1.5–2 m thick sequence of horizontal subparallel layers. The horizontal layers may represent Holocene eolian deposits and various pedogenic horizons. The State Road Pond core (Bishop et al., this volume, chap. 10: fig. 10.5) provides the nearest ground truth and includes a laminated sand at 2.5 m depth containing heavy minerals. This laminated heavy mineral–bearing sand overlies 15 cm of muddy sand. This could be an overwash fan deposit over a muddy swale or marsh. The depth is compatible with that of the proposed overwash horizon described in the GPR profile above.

Part of an east to west GPR profile (fig. 11.7B, lower profile) from Seaside Dock to the dock at Walburg Creek also shows three radar facies that may be interpreted as lower marsh to offshore clay-rich facies, middle shore or beach facies, upper washover and eolian facies with superimposed pedogenic features, similar to those described above. An additional interesting feature is shown between 650 and 655 m, just west of Jct. 17. An apparent normal fault with ~0.2 m displacement is observed cutting the upper pedogenic reflector, dropping strata on the west side of the fault. The sharp break in the upper pedogenic reflector favors a relatively hard, brittle character (humate cement?) for this feature. The presence of high-angle diffractions shown in fig. 11.7B are common and may be products of constructive interference related to diffraction hyperbolae; however, the spatial relationship with a fault and specific occurrences that cannot be traced to hyperbolic reflections favor mineralized joints in this profile segment. An iron oxide filled joint was observed in core 1 collected by Vance and students as part of a research project (Ferguson et al., 2009) near Gator Pond. Joints have also been recognized at Yellow Banks Bluff (Bishop and Rich, personal commun.).

The middle and upper radar facies thin dramatically to less than 3 m toward the west side of the island. Figure 11.8A (upper profile) shows well-developed cross beds produced by westward flowing currents. The underlying sediments are either clay rich and/or water saturated.

On portions of the King New Ground Road profile west of Jct. 45, the GPR signal was limited to less than 5 m depth. This is probably a result of high water table (estimated at ~2.4 m depth from a drainage ditch observation during GPR survey) and/or a greater proportion of clay-rich sediment near the surface. This region of limited signal return and relatively shallow water table approximately coincides with the distribution of Mandarin-Rutledge soils and former freshwater wetlands (Hayes and Thomas, 2008). Similar poor signal return is observed on GPR profile OMP2-07 on Savannah Road between jcts. 71 and 80, again approximately coincident with the central swale (Thomas, 2008) or Central Depression (Bishop et al., 2007; this volume, chap. 3: fig. 3.2) and Mandarin-Rutledge soil distribution.

An east to west GPR profile (fig. 11.8B, lower profile) from Magnolia Bluff to Jct. 13 to the west side of the island via North Beach Road also

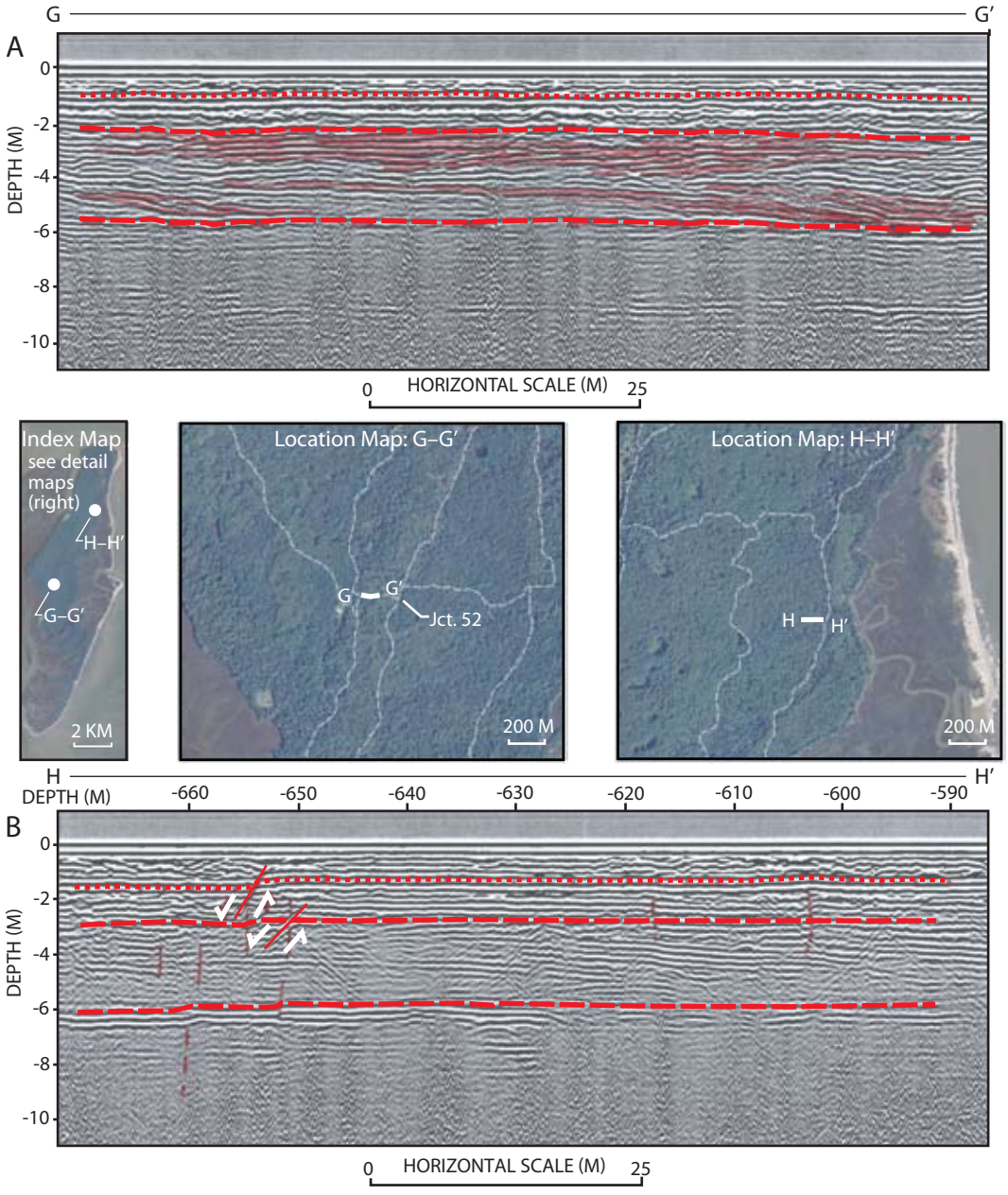

Fig. 11.7. **A,** Profile G–G′: SW-NE segment of 100 MHZ profile OMP2-07 between jcts. 52 and 71, with heavy dashed highlights separating upper, middle, and lower radar facies. Profile illustrates the sharp, persistent basal reflectors of lower facies observed under much of the island and tangential contact between middle facies reflectors and lower facies reflectors. Dotted highlight marks the pedogenic/humate reflector within an upper facies dominated by horizontal to subhorizontal reflections. **B,** Profile H–H′: W-E segment of 100 MHz profile OMP5-07. Note normal faults with ~0.2 m collective displacement cutting the humate reflector (dotted highlights). Arrows indicate relative motion. Dashed highlights separate lower, middle, and upper radar facies (aerial image source USDA, NAIP 2005).

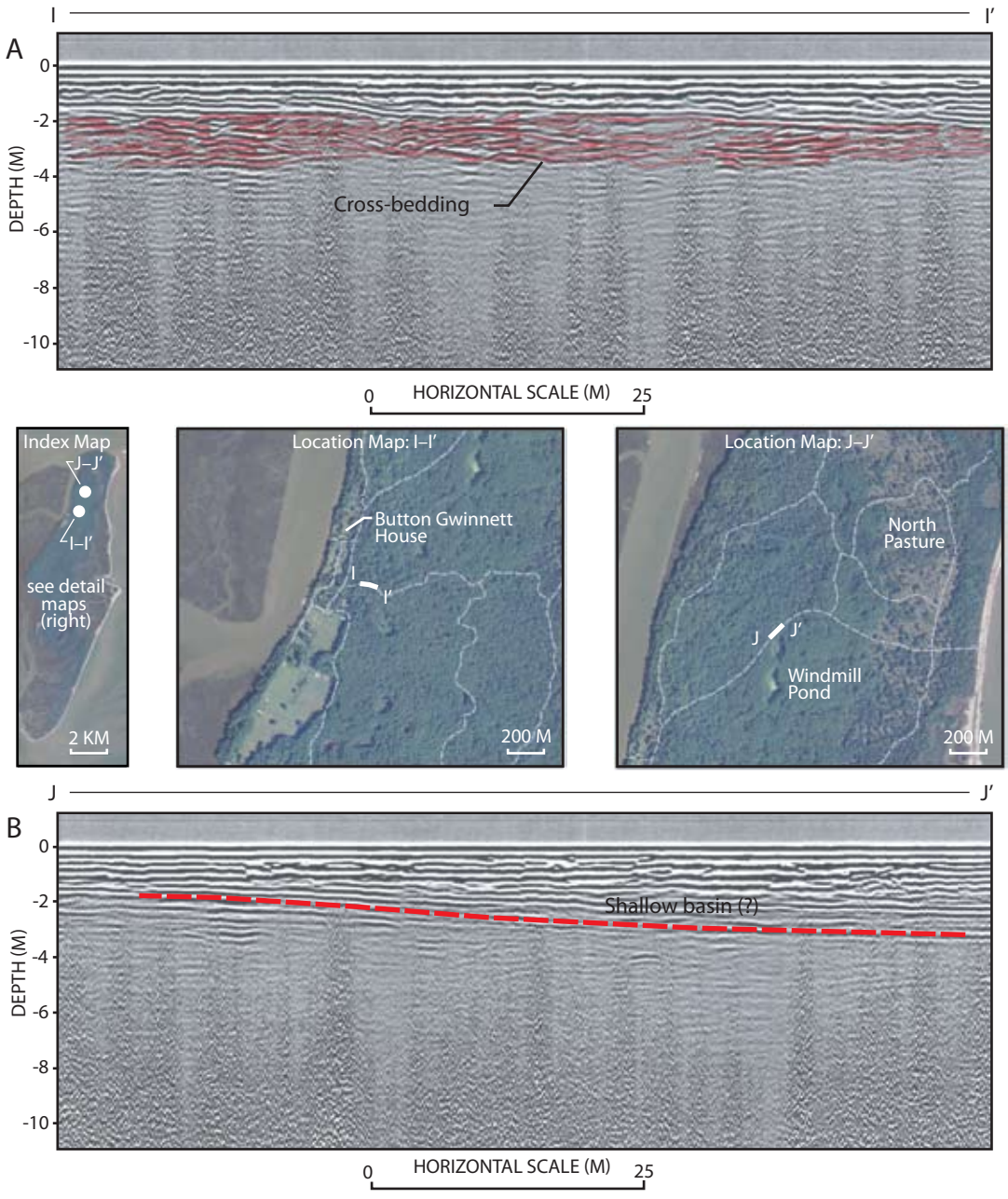

Fig. 11.8. **A,** Profile I–I′: NW-SE segment of 100 MHz profile OMP5-07 from west flank of Central Depression. Note well-developed cross beds (highlighted) limited radar penetration. **B,** Profile J–J′: SW-NE segment of 100 MHz profile OMP6-07 along North Beach Road, in the Central Depression, suggests western margin of a shallow basin. Poor signal return suggests wet sediments and/or composition rich in clay and organic components (aerial image source USDA, NAIP 2005).

exhibits weak signal return in areas that coincide with the former wetlands of the Central Depression. The region is marked today by ponds, marshes (natural and modified—Royce Hayes, 2009, personal commun.), and hydric soils and vegetation such as river cane (*Arundinaria gigantea*) that favor a shallow water table. A substantial marsh or lake probably existed in the vicinity of Windmill Pond as 100 MHz radar profiles show strata dipping gently inward to form a shallow basin cross section over a 425 m profile segment. The thickness between the lower part of the radar-visible basin and overlying horizontal reflectors suggests up to 2.5 m of sediment accumulated locally in these freshwater wetlands. The sediment accumulations and wet nature of the ground make these excellent sites for future vibracore exploration. The 250 MHz profile (fig. 11.9A, upper) shows a higher resolution view of the western margin of the basin with numerous offset reflections that suggest either fault control of basin formation or fault development in response to the subsidence that formed the basin.

The higher, drier ground east of the Central Depression yields excellent radar signal return for depths of ~7–8 m with the 100 MHz antenna revealing the persistent basal reflectors associated with the lower horizontal planar facies (fig. 11.9B, lower). The major radar surfaces bracket a middle facies of strata inclined toward the east, with the lowest beds tangential to the basal facies beds. The upper facies is dominated by subhorizontal planar reflectors. Identification of true dip direction requires a right-angle view, and figure 11.10A, upper, from a south to north profile between Jct. 13 and Jct. 10, provides this perspective. Note that nearly all beds appear parallel in this view, indicating a north-south strike for the beds of the middle facies.

Figure 11.10B (lower) illustrates the sharp contrast between the lower and middle facies and the vertical and lateral changes in the character of bedforms in the middle facies. Note the eastward dip of the lower strata within the middle horizon or facies versus the westward inclination of overlying cross beds or foresets. Figure 11.11A (upper) is the adjacent profile segment to the west. The GPR signal is limited to ~5 m depth suggesting mud, organic sediments, and/or high water table. Are the west-dipping reflector sands overriding marsh deposits or is the water table simply higher in this location?

The basal reflectors of the lower facies cannot be traced continuously across the Central Depression; however, the collective profile segments that do show this marker indicate thinning of the overlying sand toward the west. Figure 11.11B, lower, is a segment of profile OMP6-07 located approximately 80 m east of Jct. 64. The profile exhibits an undulating basal reflector with a middle facies that appears to thin westward. This profile terminated in the pasture on the north side of the barn west of Jct. 64. At that point a strong basal reflector was observed at ~3 m below the surface and overlying strata appear horizontal, requiring either erosional thinning or markedly reduced deposition of overlying sands. Determining whether the westward thinning is a product of erosion or reduced deposition of sand is important to both archaeological and geological exploration of the island. Interpretation of missing strata also assumes that the basal reflector on the east and west side of the island is essentially the same unit. The validity of this assumption requires further testing and the proposed (Bishop et al., chap. 3, fig. 3.3) evolution of the island demands it. The surface of the basal reflector undulates to the west and east of Jct. 64, and features that can be interpreted as faults (fig. 11.12A, upper) are present at 1980 m on the profile.

Profile OMPU-06 strikes east to west in a transect from Jct. 10 to Jct. 61, then southeast to northwest from Jct. 61 to Jct. 60. Profile segments (fig. 11.12B, lower: 31–295 m) near Jct. 10 are complex with a thick sequence of sandy sediment that contains three to four distinct radar surfaces. The basal reflector that appears to continue westward is the radar surface at ~8 m depth. It appears to have sand beneath it here because the signal penetrates farther below the surface. The 31–119 m segment shows the upper pedogenic reflector at 0.8–1 m overlying largely subhorizontal strata with local cross-bedding and trough features. The surface between 3.2 and 4 m and appears to be disconformable (at least locally; see scour at 62 m) and overlies a rippled or undulating surface that is best developed along profile segment from 65 to 100 m. The poor radar signal below the rippled surface suggests high clay and/or organic sediments or high water content. This surface may be the top of the Pleistocene if the interpretations and dates of Vento and Stahlman (chap. 4, this volume) are correct. This intensively burrowed surface exposed in the lower 1.5 m of Yellow Banks Bluff has been studied in detail by Martin and

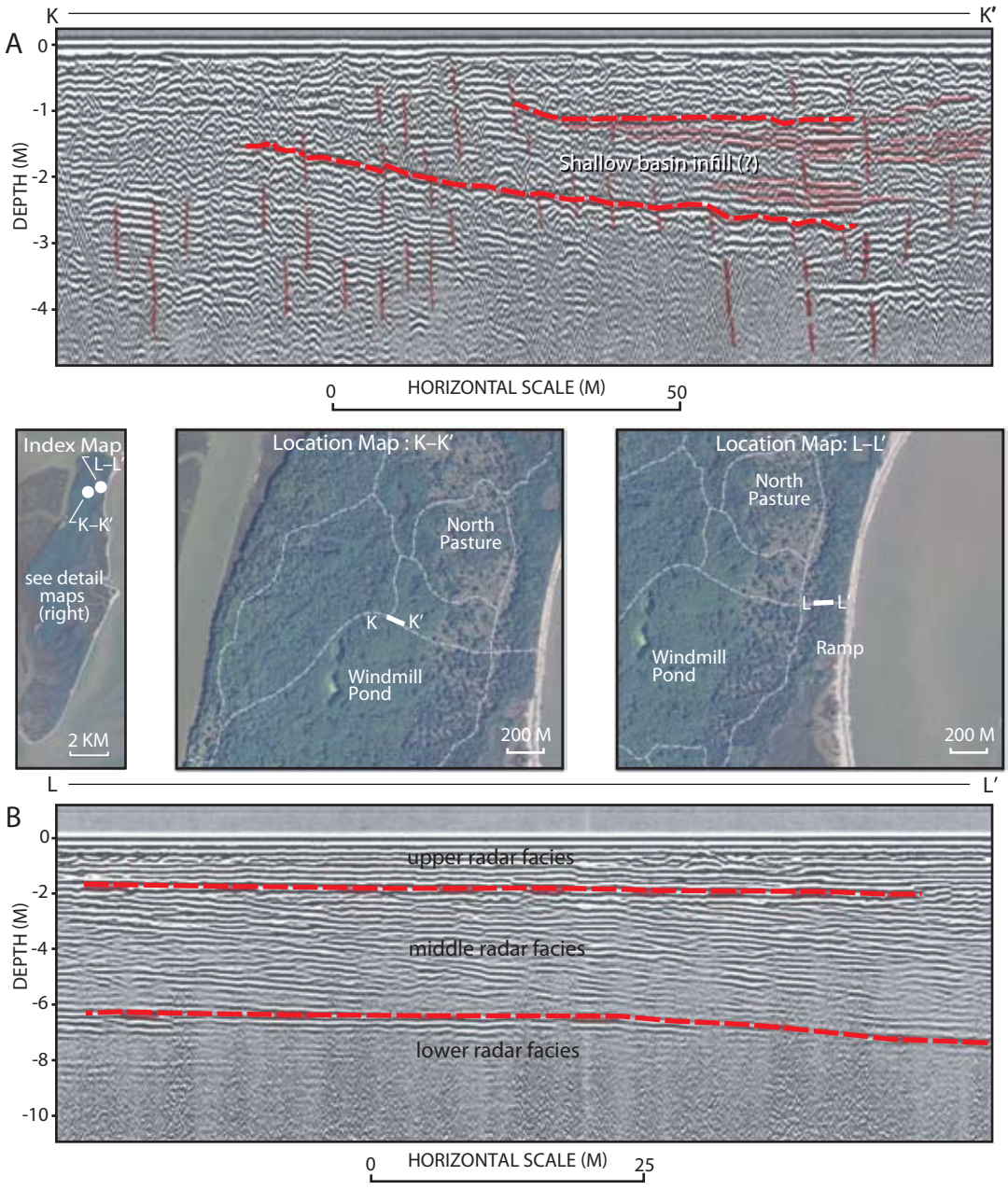

Fig. 11.9. **A,** Profile K–K′: W-E segment from 250 MHz profile OMP4-09 east of the profile J–J′ (fig. 11.8) in the Central Depression. Highlights on basin bottom and numerous offsets suggesting small faults. Horizontal reflections suggest infilling of the basin and a good site for vibracoring. **B,** Profile L–L′: W-E segment from 100 MHz profile OMP6-07, east of the Central Depression near Jct. 13, revealing horizontal planar bedforms of lower radar facies, a middle horizon radar facies of bedforms (radar elements) inclined and tangential to the lower horizon, and an upper radar facies of horizontal to subhorizontal elements (aerial image source USDA, NAIP 2005).

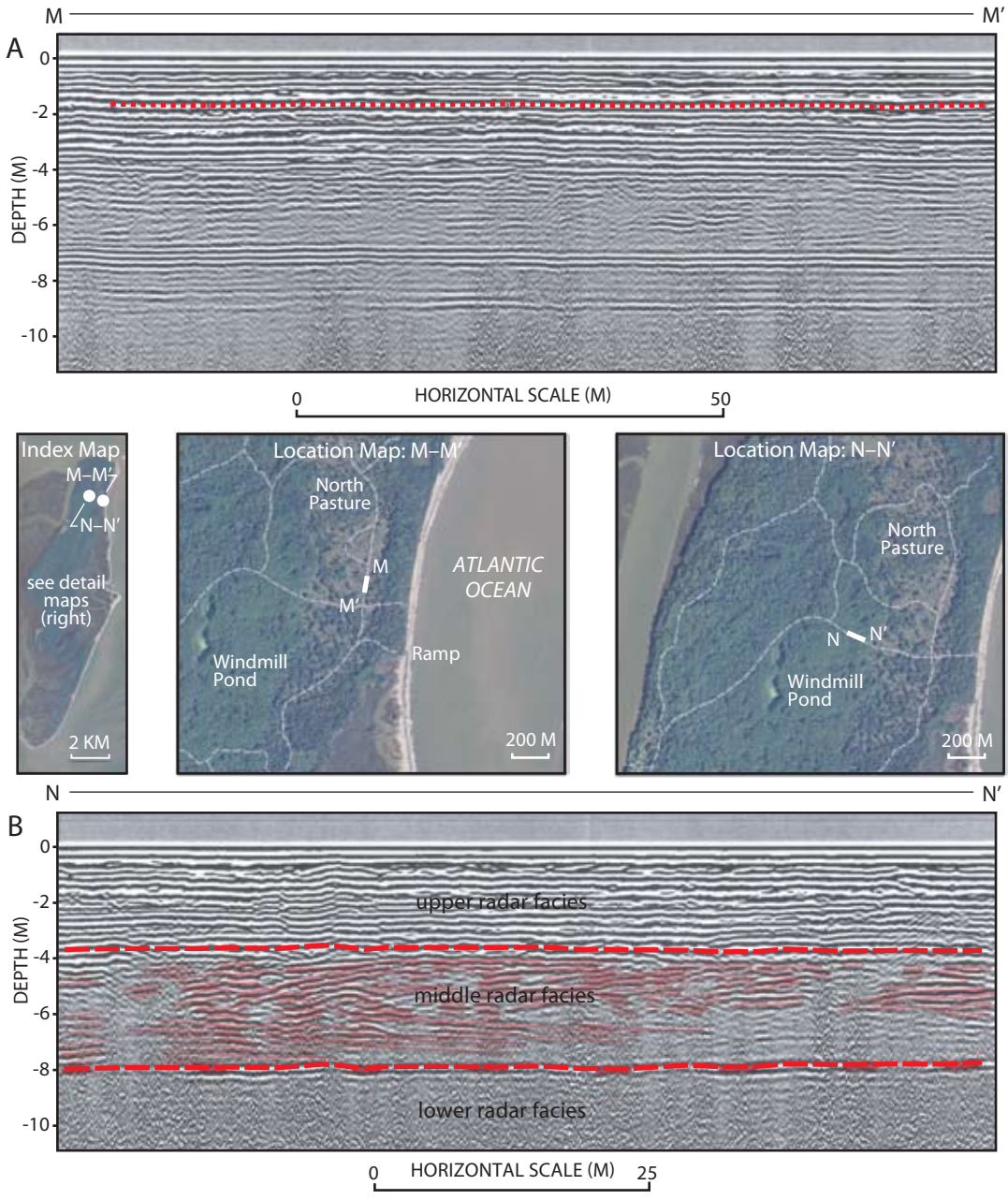

Fig. 11.10. **A,** Profile M–M′: N-S segment of 100 MHz profile OMPT-07 between Jct. 13 and Jct. 10 indicates north-south strike for strata of middle horizon or facies. Compare to E-W transect in profile L–L′ (fig. 11.9). **B,** Profile N–N′: W-E segment from 100 MHz profile OMP6-07 showing lateral changes in attitude of middle facies radar elements or bedforms (highlighted). Basal reflector marking top of lower facies is at lower dashed line. This segment joins Profile O–O′ (fig. 11.11) along the eastern flank of the Central Depression (aerial image source USDA, NAIP 2005).

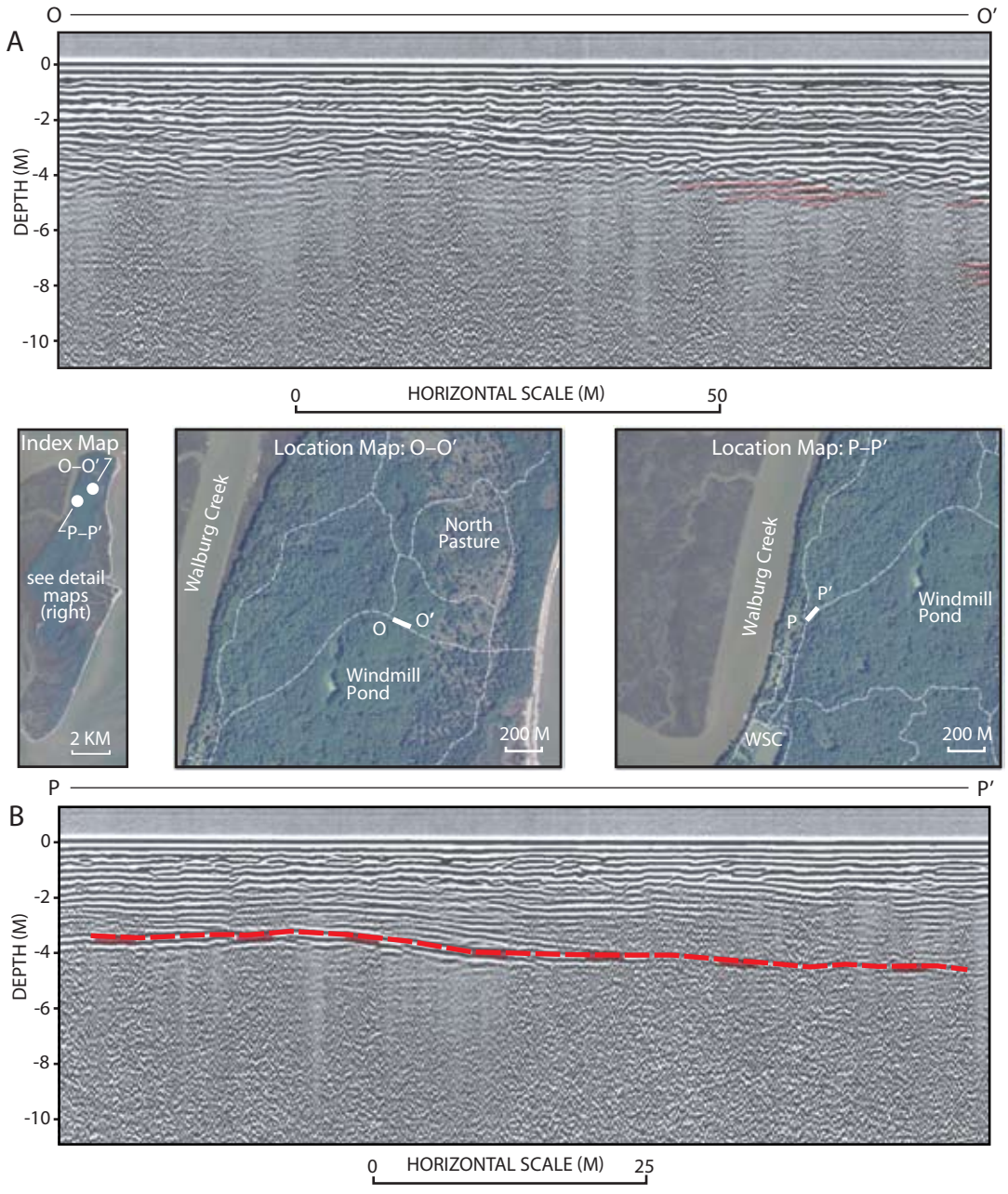

Fig. 11.11. **A,** Profile O–O′: Adjacent segment from same W-E profile as Profile N–N′ (fig. 11.10) along the eastern flank of the Central Depression. Note the limited depth of GPR signal penetration and return. These zones may be sites of former marshes or ponds with poor signal return due to more clay, organic components, and/or water. **B,** Profile P–P′: SW-NE segment from 100 MHz profile OMP6-07 showing undulating surface of basal reflector (highlights) with much thinner overlying sands in contrast with the eastern side of island (aerial image source USDA, NAIP 2005).

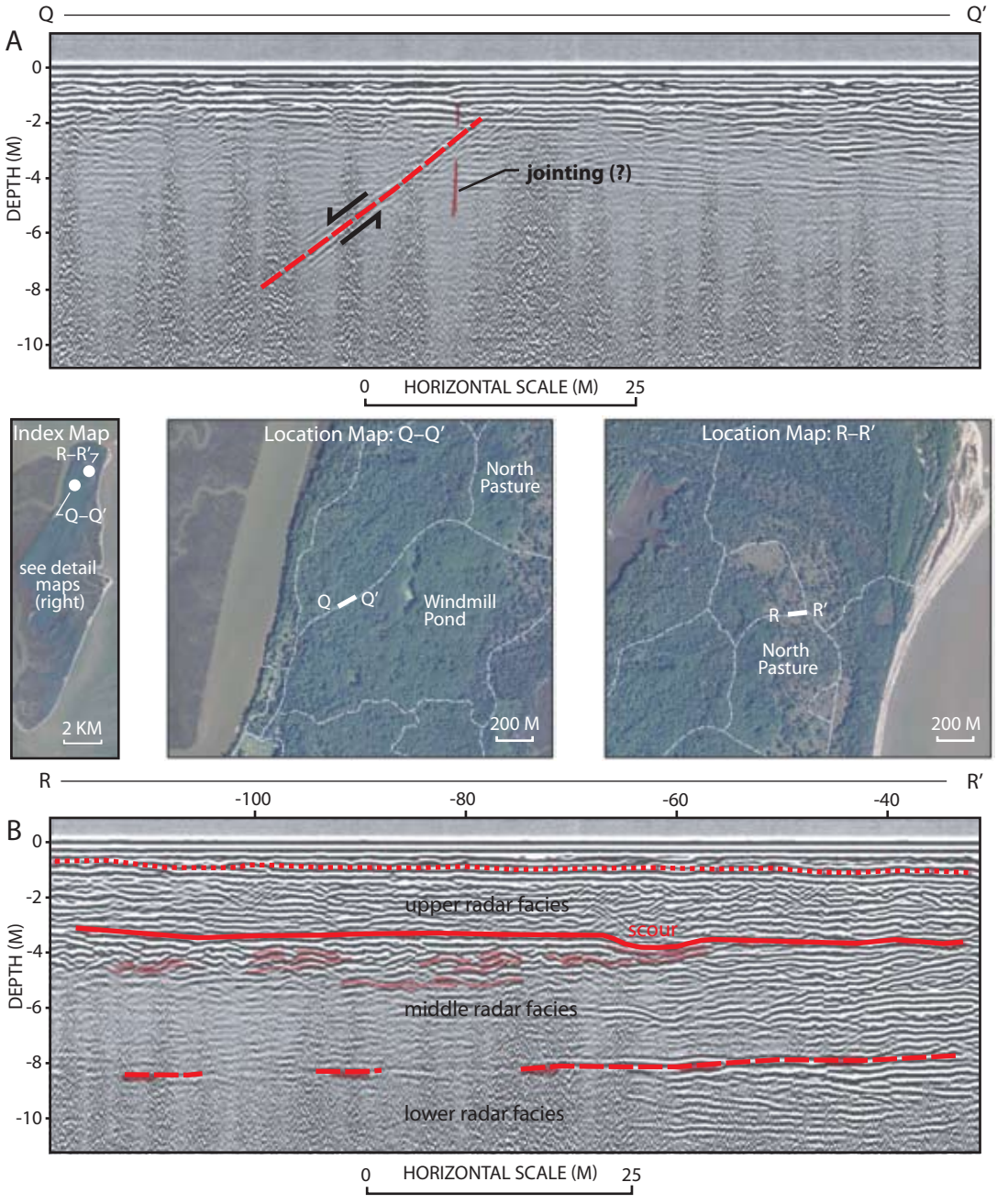

Fig. 11.12. **A,** Profile Q–Q′: SW-NE segment from 100 MHz profile OMP6-07 showing thin sands and steeply dipping reflections or diffractions suggesting a small fault and/or joints. Poor signal return suggests a higher water table or more clay and organic components. **B,** Profile R–R′: W-E segment from 100 MHz profile OMPU-07 showing pedogenic/humate reflector (dotted highlight) and intense reflectors (dashed highlight) at ~3 m depth overlying a possible marsh (zone of poor signal). Scour (62 m) and rippled surfaces (65–100 m) are highlighted (aerial image source USDA, NAIP 2005).

Rindsberg (chap. 5, this volume) and interpreted as washover fans and associated sediments that were host to a number of organisms. Vento and Stahlman (chap. 4, this volume) describe subaerial exposure and date soil horizons developed on this surface and overlying surfaces but caution that soil horizons developed in overlying Holocene eolian deposits are not laterally continuous. The features on the inland radar profiles could certainly be interpreted as overwash into a marsh or large swale pond if the zones of poor signal return represent clay or organic-rich sediments. If this can be verified with a core, the GPR would be a valuable tool for guiding selection of additional core sites to areas that would yield organic sediments suitable for ^{14}C dating and palynology studies. The north-south leg of profile OMP1-09 (fig. 11.13A, upper) intersects profile OMPU-07 at Jct. 10, providing a right angle view. Strata appear parallel to subparallel in this area, indicating a general north-south strike of the beds. The intense reflector between 3 and 4 m depth is apparent over a zone of poor signal return. The southwest-northeast leg of the profile (fig. 11.13B, lower) illustrates a strong reflector between 4 and 5 m depth (~ top of Pleistocene?) overlain by cross-bedded strata (eolian?) with a sharp local boundary between cross-bedded layers. At ~5.5–7.5 m depth a large wedge of sediment terminates in foreset beds that dip into the "soft" signal zone (marsh?). Is this a cross section of a thick Pleistocene storm washover filling in the marsh behind a breached dune ridge? The cross-sectional geometry of the radar elements/bedforms is certainly compatible with such an interpretation. The beds truncate the underlying strata and dip into the proposed marsh area, leveling out at the top of the sediment wedge as it overrides the marsh. Following this interpretation, the lower dipping strata along segment 1190–1370 m of profile OMP1-09 (fig. 11.14A, upper) may represent ridge and swale systems truncated by overwash and eolian deposits.

The individual horizons described above are very difficult to trace westward since the strata become parallel as the profile turns northwest. Distinctive radar surfaces are limited to the upper pedogenic reflector and basal reflector(s). The basal reflector is about 5 m below the surface in the more "compressed" section near Jct. 60, suggesting that the proposed Holocene base is less than 2 m deep in this area. Vibracores obtained in a transect (Ferguson et al., 2009) between Jct. 60 and Jct. 10 exhibit multiple humate or iron oxide horizons and lack obvious bedding features or notable structure above 2 m. Heavy minerals concentrated in laminations define bedding below 2 m depth and concentrations may reach 5%–10% in zones a few centimeters thick. Hand auger exploration at Jct. 10 extracted white "sugar sand" at depths of 3 m. The collective auger and vibracore data suggest that the Holocene eolian deposits of the upper facies thin westward from 3 m near Yellow Banks Bluff to 2 m or less on the central and western side of the island. This interpretation is supported by recent profiling (OMP4-09) with the 250 MHz antenna.

An additional feature of interest occurs between 645 and 560 m on the northwest portion of profile OMPU-06 (fig. 11.14B, lower). It shows the faint but well-developed outline of a wedge of sediment thinning to the east or southeast above a basal reflector. The sediment wedge displays foresets dipping in the same direction. Could this be the margin of a Pleistocene tidal delta or bar building toward the south or southeast over muddy sediments (see this volume, chap. 3: fig. 3.3)? The deep water table and relatively high elevations at the northeast end of the island favor strong radar penetration and signal return. There also seems to be better radar penetration of the lower facies in the northern part of the island, suggesting less clay and more sand. This may reflect closer proximity to the major sand supply (Bishop et al., this volume, chap. 3).

STRUCTURAL FEATURES AND ISLAND HYDROLOGY

Radar profiling on St. Catherines Island reveals several subsurface features with a synformal appearance in the cross-sectional profile view. The first example was discovered on the north end of the island on profile OMPU-06 (fig. 11.15A, upper) on the northwest-southeast profile leg along the road southwest of Gator Pond. The synformal features lack associated antiforms and the general passive margin tectonic setting does not favor major horizontal compressive stresses of the type that generate such features, so it should be safe to eliminate compressional folding as a realistic possibility. The more realistic possibilities for generating such structures include a filled fluvial or tidal channel, differential compaction over some local high porosity sediment—possibly over a deeply buried chan-

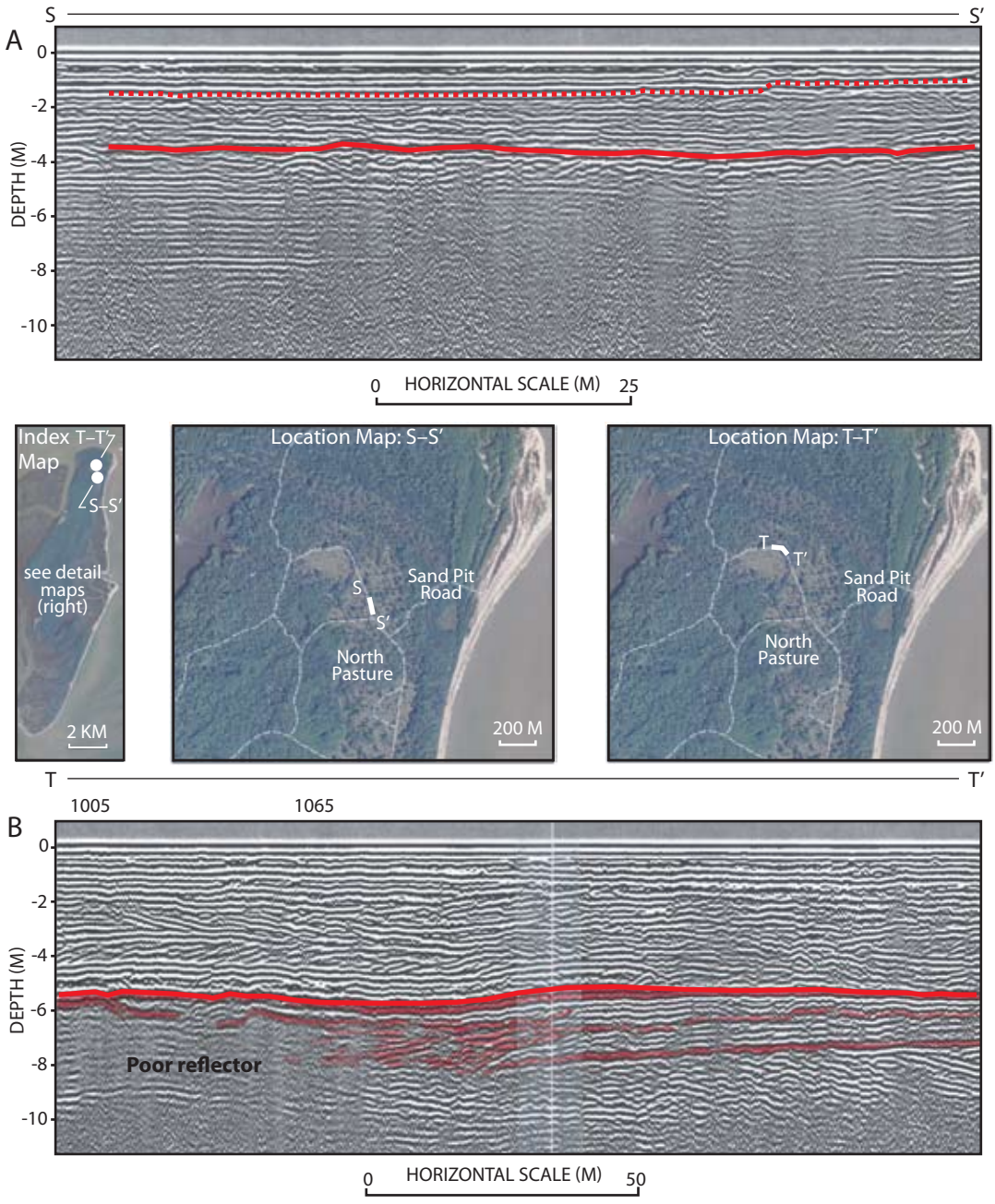

Fig. 11.13. **A,** Profile S–S′: N-S profile segment from 100 MHz profile OMP1-09 providing a right-angle view of sequence shown in profile R–R′ (fig. 11.12). Note pedogenic/humate reflector (dotted highlight) and the intense reflector (solid highlight) above marsh (?) deposits. Horizontal bedforms indicate N-S strike of strata by comparison with profile R–R′ (fig. 11.12). **B,** Profile T–T′: W-E-SE segment of 100 MHz profile OMP1-09 showing highlighted reflections/strata interpreted as large washover fan building into and over a marsh or swale pond (area of weak reflections between 1005 and 1065 m). Note well-developed cross-stratification in sequence above marsh and washover (aerial image source USDA, NAIP 2005).

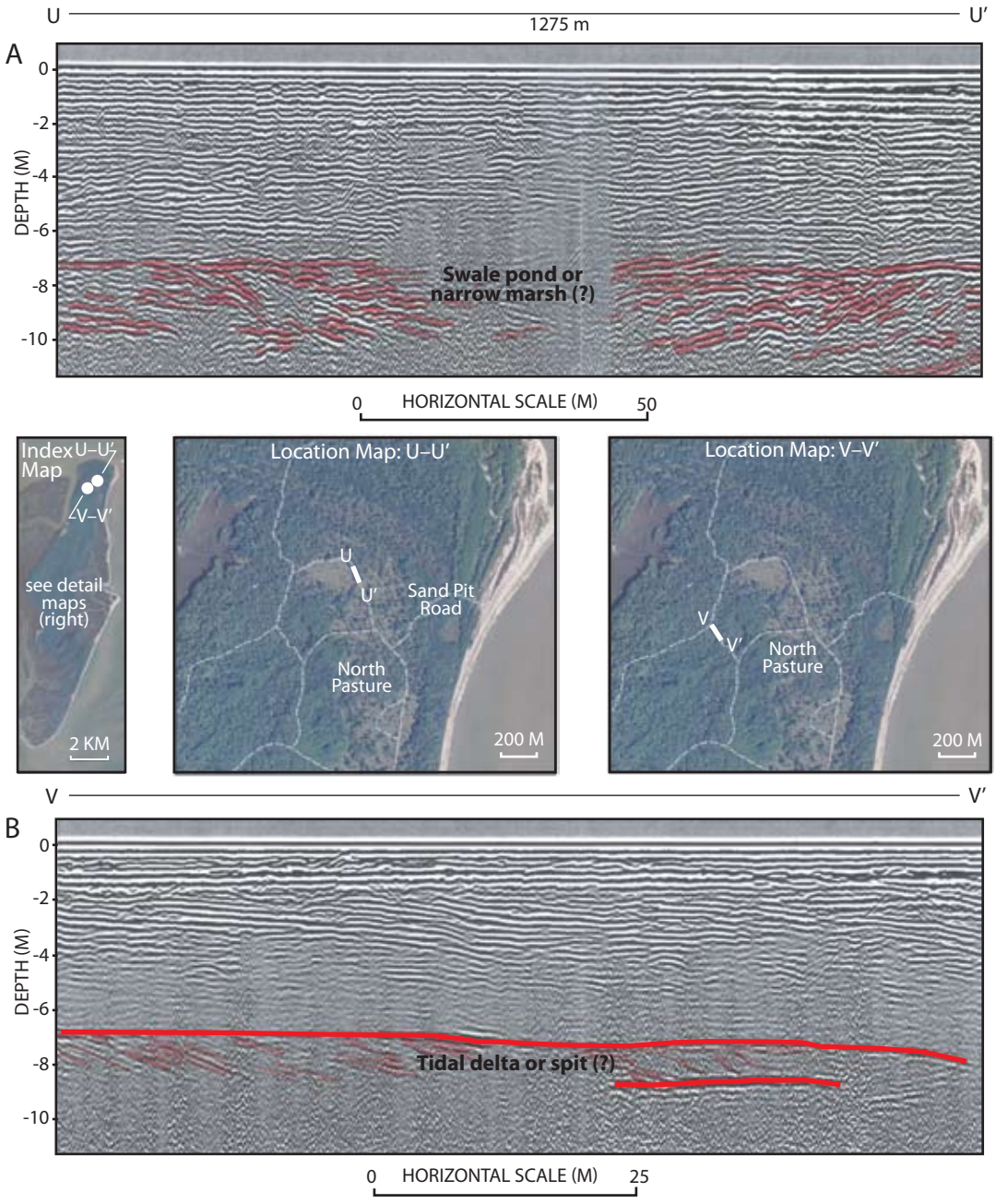

Fig. 11.14. **A,** Profile U–U′: NW-SE segment from profile OMP1-09 showing possible swale pond or narrow marsh (~1275) with adjacent sandy strata dipping into and filling (?) swale. Another possibility might be a deep runnel in a beach system. **B,** Profile V–V′: NW-SE segment from 100 MHz profile OMPU-07 illustrating foreset bedforms in a layer thinning toward the east or southeast. Could this be the toe of a tidal delta or spit (aerial image source USDA, NAIP 2005)?

nel, or the local collapse of strata into an underlying sinkhole or solution cavity. A narrow graben generated by tensional tectonics is another possibility. If the feature is a channel, there should be truncation of strata along the margin produced when the current eroded the underlying strata. There could also be some high-energy bedforms within the channel. Some possible truncation may have occurred in the upper 2 m along the southeastern margin of the Gator Pond structure. The general appearance of the feature and the thickness of bedforms suggest that underlying strata sagged ~2 m. This appears to have occurred after the development of the sharp reflecting horizon (humate reflector?) marked on the profile. The feature acted as a basin or channel collecting sediments that eventually filled in the depression. The sag feature approximately coincides with a surface topographic low that drains from Gator Pond toward the new pond at the old Crane Yard. The upper 1.2 m of sediment in the profile trough is mostly road fill across the depression.

Dissolution of carbonate rock at depth is another means of generating these sag structures. Carbonate rocks exist at relatively shallow levels beneath some of the barrier islands. Drilling on Cumberland Island encountered carbonate rock and some solution cavities at ~17–24 m below the surface (McLemore et al., 1981) in Pliocene strata. The Upper Brunswick Aquifer (Miocene) is another dissolution candidate with local carbonate units at depths between 30 and 60 m along parts of the coast. The Floridan Aquifer is a deep candidate at ~130 m. Solution cavities and collapse structures or sags localized by joints or faults are a realistic possibility and small displacement faults appear on some of the profiles. The Gator Pond sag feature is being investigated by Vance, Rich, and Bishop working with an undergraduate research team (Ferguson et al., 2009) using a transect of 10 vibracores to obtain shallow stratigraphic control and samples for palynology and sedimentology.

Profile OMP1-09 encountered another sag structure north of Gator Pond (fig. 11.15B, lower) with ~5 m of apparent subsidence along the sag center and numerous potential faults. This profile was conducted along the road that loops around the north end of the island from Jct. 60 to Jct. 10. Potential fault or joint control on development of these sag structures will be tested with additional east-west profiles between the Gator Pond sag and this sag to see if the structures are isolated or part of a continuous trough or graben. A profile conducted in July 2010 indicates the sag shown in fig. 11.15B extends to the southeast.

Profiles OMPR-07 and OMPK-06 encountered another sag structure below State Road in the vicinity of State Road Pond. Figure 11.16A (upper) from profile OMPK-06 is a shallow-window 100 MHz profile crossing this sag structure. The scale of the shallow time window reveals multiple reflection offsets suggesting small faults associated with the structure. This feature appears to result from 1.5–2.5 m of subsidence in the deeper portions. The sag feature deflects strata to depths of 8 m and is similar to the others in the lack of obvious truncating features indicative of channels. An additional sag feature was discovered on profile OMP2-07 (fig. 11.16B, lower) on Savannah Road between Jct. 80 and the creek to the east. The sand is about 5 m thick and the basal reflector is depressed at this locality.

The sag features appear to have formed by a combination of soft sediment deformation and local brittle failure (of cemented zones) in the form of numerous small-displacement faults. Additional profiles around known sags will document the extent of individual structures and determine if these features are isolated basins or linear troughs. Elongate, troughlike structures would suggest strong control by deeper faults or joints. The occurrence of these features along the Central Depression and present wetlands favors a strong link to island hydrology. The Late Archaic sites along freshwater marsh or lacustrine habitat and the historical accounts of the spring-fed streams and meadows (Hayes and Thomas, 2008) certainly indicate artesian flow. The Floridan artesian aquifer is well below the surface in this area; consequently, the overlying strata must be penetrated by natural conduits such as faults or joints or by man-made conduits (wells) to allow this water to reach the surface. The sag structures may mark areas in which faults or joints have localized dissolution in carbonates at depth or there may have been deep structural subsidence expressed as minor faults and sags at the surface. Either mechanism would provide surface access to the artesian aquifer and the preindustrial potentiometric surface would have produced impressive artesian flow (Krause and Gregg, 1972; Hayes and Thomas, 2008).

Although the artesian springs no longer flow on St. Catherines Island, the importance of these potential hydrologic conduits along the Central

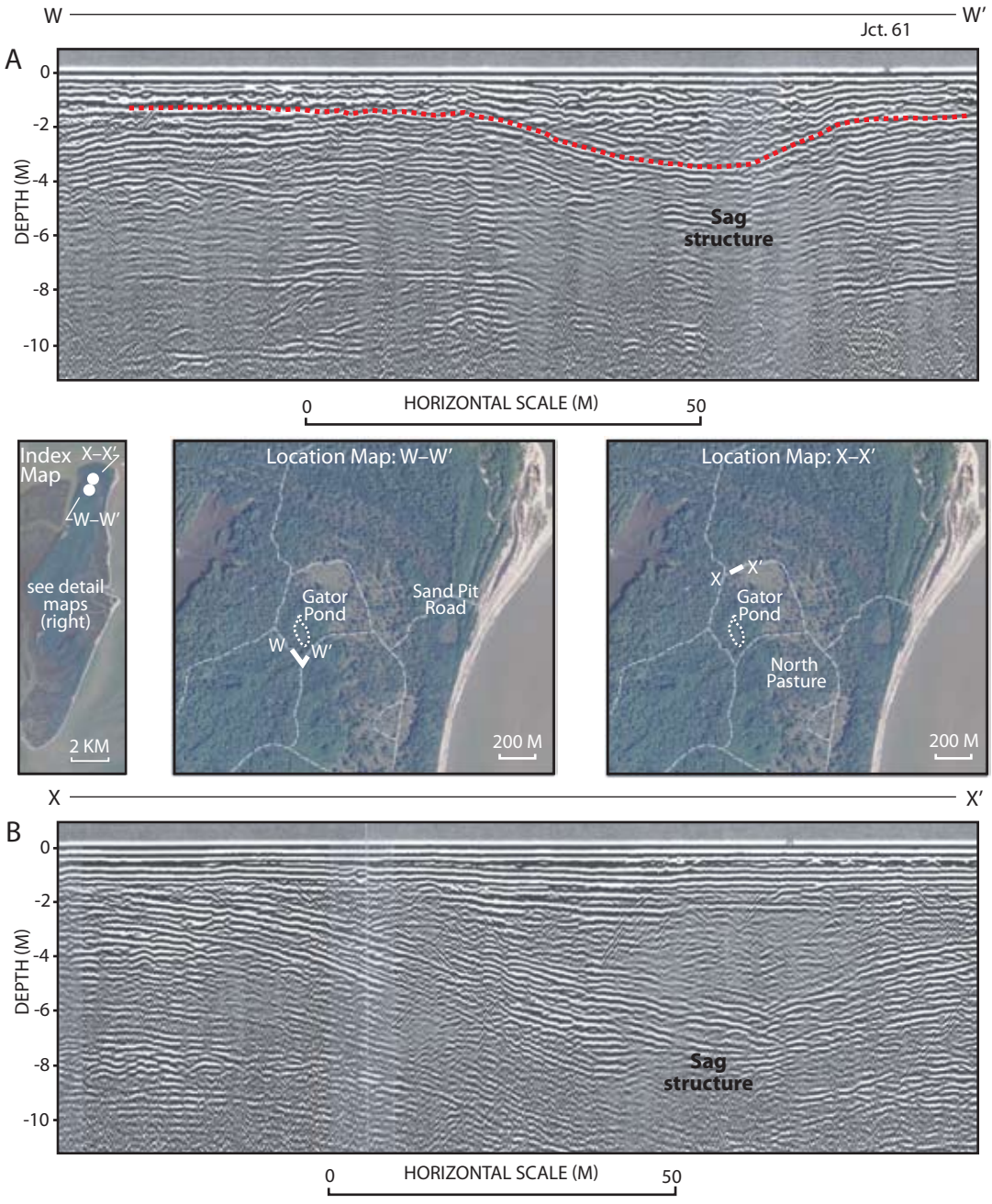

Fig. 11.15. **A,** Profile W–W′: Segment (NW-SE-NE) from 100 MHz profile OMPU-07 showing sag structure on southeast side of Gator Pond. Jct. 61 is at 454 m on the profile. Dotted highlight marks pedogenic/humate reflector. **B,** Profile X–X′: Broad sag structure north of Gator Pond structure, on SW-NE segment of 100 MHz profile OMP1-09 (aerial image source USDA, NAIP 2005).

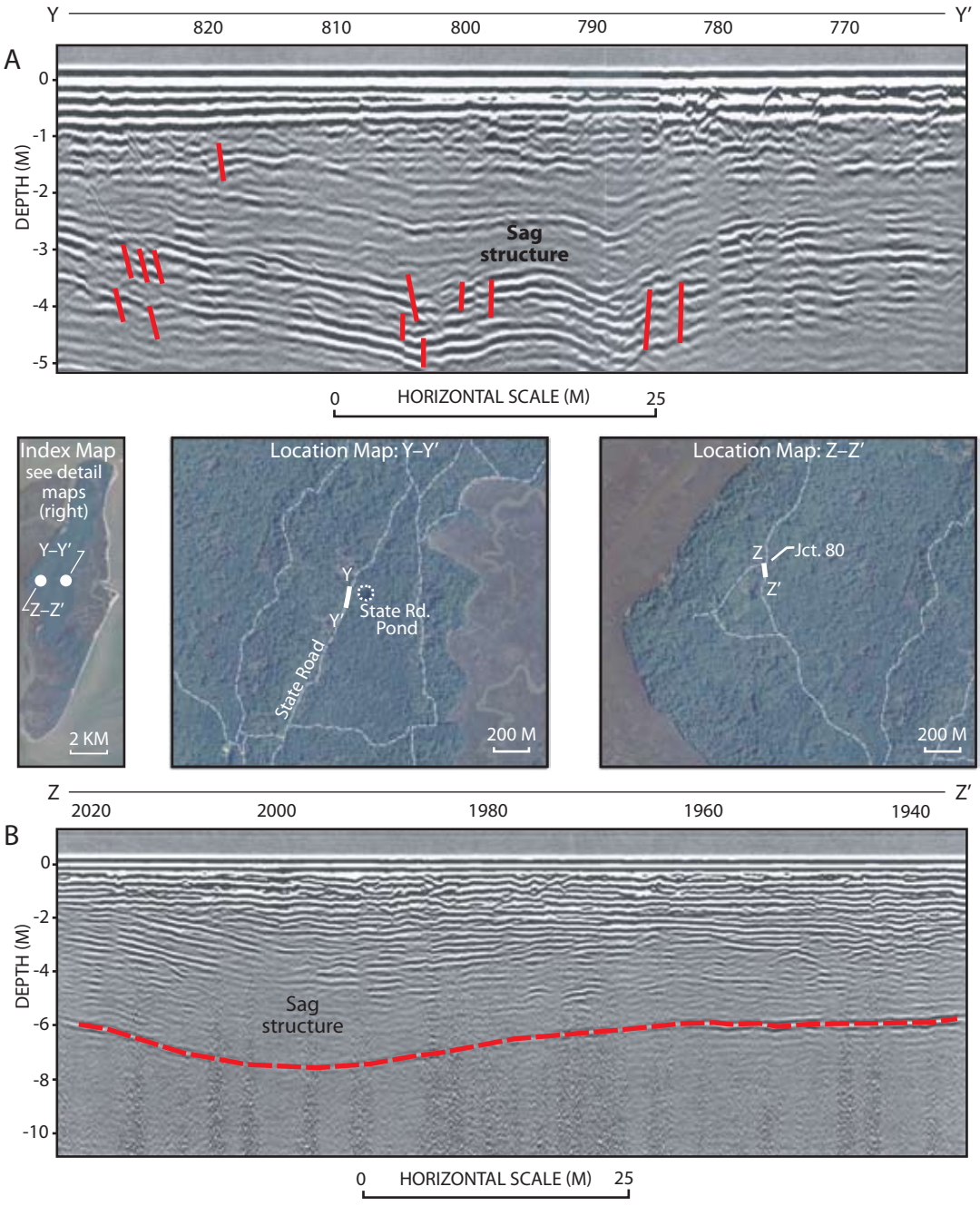

Fig. 11.16. **A,** Profile Y–Y′: view of upper portion of sag structure west of State Road Pond. From N-S segment of 100 MHz profile (shallow window) OMPK-06 along State Road. Highlights on small faults suggested by displacement and deformation of reflecting horizons at 806 m, 789 m, and 826 m. **B,** Profile Z–Z′: sag feature on NW-SE segment of 100 MHz profile OMP2–07 between Jct. 80 and the creek to the east. Note the deflection of the basal reflector (highlighted) (aerial image source USDA, NAIP 2005).

Depression should not be minimized. Sea level is rising and there is potential for hydrologic communication between the shallow and deep aquifer system via fractures and solution cavities. The saltwater intrusion that affects aquifers of the postindustrial coastal plain of the southeastern United States could contaminate the primary freshwater resource of the island if saltwater enters the same fractures that once produced artesian springs. The continued exploration of the strata and structure of the Central Depression is important for better understanding of critical island hydrology and to better understand the general geological evolution and the role of geology as a major influence on the anthropological trends or patterns of habitation and foraging (Thomas, this volume, chap. 1).

SUMMARY

GPR provides an excellent tool for noninvasive exploration of relatively shallow (<20 m) stratigraphy, geological structures, and some biogenic structures in rock and sediment. Although the electromagnetic waves of GPR are limited by the presence of clay and saltwater, the relatively thin sand-dominated sediment package that composes much of barrier islands makes GPR an extremely useful geophysical tool for both geologists and archaeologists. Varied combinations of antennae, instrument settings, survey systems, and software programs can be adapted for geological reconnaissance of stratigraphy and structure or high-resolution exploration of heavy mineral laminations in beach sediment, biogenic features (e.g., sea turtle nests), and anthropogenic features such as the island shell ring sites or Mission Santa Catalina de Guale (Thomas, 2008).

It is emphasized that depths shown on the radar profiles are not "absolute truth" and can be shifted significantly by adjusting average velocity used in the GPR software programs. The relative stratigraphic position of the features and interpretation of radar elements as specific bedforms or an association of bedforms is important in the effort to correlate the geophysical signature with available ground truth and apply these interpretations to understanding the structure and evolution of the island. Interpretation of observed radar elements bounded by major radar surfaces and or marked changes in the form of elements allowed organization of much of the island into three major facies or horizons. The lower facies is characterized by horizontal parallel-to-subparallel elements or bedforms that probably represent clay-rich, relatively low-energy sedimentary environments. The lower facies is overlain by a sand-dominated middle facies exhibiting sigmoidal clinoform radar elements or bedforms typical of beach ridge successions produced by prograding (regressive) systems (Johnston, Thompson, and Baedke, 2007). The middle facies thickens toward the northern end of the island and thins to the west. Poor radar penetration and signal return along the Central Depression and thinning of sand to the west prevent confident correlation of the middle facies to the west side of the island. The middle facies is overlain by an upper facies that includes radar elements or bedforms interpreted as overwash and eolian deposits. Both planar and trough cross beds are suggested and these forms yield to dominantly horizontal to subhorizontal planar elements toward the surface. A common, persistent reflector observed between 0.8 and 1.5 m seems to coincide most closely with humate or iron oxide concentrations.

There are definite local features in the northeastern subsurface that may be correlative with the washover fan horizon described by Martin and Rindsberg (chap. 5, this volume) and the soil horizons described by Vento and Stahlman (chap. 4, this volume). Much of the island core exhibits about 1.5–2 m of surficial sand that shows up on the radar profiles as largely subhorizontal reflections with a superimposed humate/iron oxide reflector. This surficial portion of the upper facies may represent in part an extensive Holocene eolian cover. Much of the underlying middle facies strata can be interpreted as Pleistocene beach facies truncated by overwash fans and dunes with local swale ponds or marshes. These swales or marsh trends could be delineated in the subsurface with additional across-axis 100 MHz profiles coupled with coring or auger work for ground truth and some additional higher resolution 250 MHz profiling.

The discovery of the South Pasture disconformity offers another area of focus for future research with a potential source of organic material for both palynological and radiocarbon dating. If the Yellow Banks Bluff soil profile dates of Vento and Stahlman (chap. 4, this volume) are accurate and the upper horizon recognized on most of the GPR profiles is Holocene eolian cover, the potential of older sites for archaeological exploration is enormous.

Much of the work described here is reconnaissance level, but led to focused research on parts of the Central Depression to explore its origin and the underlying structural and stratigraphic controls on island hydrology. The present level of research suggests that joints and faults along the Central Depression may have localized solution in underlying carbonate rocks producing surface sinks or structural sags. It is also possible that these depressions were localized by minor fault-controlled subsidence. These structural conduits probably tapped the artesian aquifer to produce the springs and freshwater wetlands known in early colonial times. These conduits could also provide saltwater access into the island core due to pervasive saltwater intrusion associated with the falling potentiometric surface of the Floridan Aquifer. Obtaining additional deep vibracores from the Central Depression, coupled with palynological analyses of organic sediment from the cores, can be teamed with additional radar profiling and continued cataloging of archaeological sites along the former wetlands margin to explore the temporal and spatial extent of the wetlands that were so important to both the geological and human history of the island.